Investigation of the synergy potential of oil and geothermal energy from a fluvial oil reservoir

Ziabakhshganji, Zaman; Nick, Hamidreza M.; Bruhn, David F.

DOI
10.1016/j.petrol.2019.106195

Publication date
2019

Document Version
Accepted author manuscript

Published in
Journal of Petroleum Science and Engineering

Investigation of the synergy potential of oil and geothermal energy from a fluvial oil reservoir

Zaman Ziabakhsh-Ganji [a], Hamidreza M. Nick [a,b], David F. Bruhn [a,c]

[a] Faculty of Civil Engineering and Geosciences, Delft University of Technology, The Netherlands
[b] Danish Hydrocarbon Research and Technology Centre, Technical University of Denmark, Denmark
[c] Helmholtz Centre Potsdam – GFZ German Research Centre for Geosciences, Germany

Corresponding author: Zaman Ziabakhsh-Ganji
E-mail: z.ziabakhshganji@tudelft.nl

Abstract

Geothermal projects, as renewable energy projects, are not economically attractive in most places of the world at the current state of development; for this reason, subsidies are required by energy and environmental authorities in order to increase the interest in such projects. In this paper, we assess and model strategies for integration of geothermal energy with oil productions of the Moerkapelle oil field in the Netherlands. To do so, numerical simulations have been employed to analyse the feasibility of a fluvial oil reservoir for the synergy potential of oil and geothermal energy exploitation. In order to implement the simulation studies, single phase and two-phase non-isothermal fluid flow modelling are utilised for the geothermal well doublet system and for water flooding in an oil reservoir (including facies heterogeneity), respectively. A series of simulations have been conducted to investigate how hot water from a geothermal reservoir beneath a heavy oil reservoir in the fluvial sedimentary system of the West Netherlands Basin can be used for Thermal Enhanced Oil Recovery (TEOR) and geothermal energy production.

This study finds that the high degree of heterogeneity in fluvial oil reservoirs could significantly affect oil recovery improvement and hence the synergy strategy. High values of a) Net to gross (N/G) b) Bottom Hole Pressure (BHP) and c) horizontal wellbore length are favourable for oil recovery. In contrast, wide horizontal wellbore spacing and oil viscosity have an adverse effect on oil recovery enhancement. Furthermore, the results display that the enhanced oil production helps to reduce the required subsidy for a single doublet geothermal project up to 100 %. Consequently, the extra amount of oil produced by utilising the geothermal energy, could make the geothermal business case independent and profitable.

Keywords: Geothermal energy; Thermal Enhanced Heavy Oil Recovery (TEOR); Heterogeneity; Net to Gross (N/G); Net Present Value (NPV).

1. Introduction

In the Netherlands there are several reservoirs that contain heavy oil with high viscosity. Some of these reservoirs are located in a porous sandstone from the Lower Cretaceous Nieuwekerk formation in the West Netherlands Basin. Most of such fields were either never developed or they have been abandoned, as they were not considered to be profitable at the time. The Moerkapelle field is a good example for such an abandoned reservoir at a depth of about 800-1000 meters (Smits 2008; EBN, 2013; Ziabakhsh-Ganji et al., 2016, 2018). Oil production from these types of reservoir needs some Enhanced Oil Recovery (EOR) method, and thermal EOR is one of the most applicable methods. Particularly, thermal EOR implemented in many projects such as steam stimulation, or cyclic steam flooding, also known as steam flooding, Steam Assisted Gravity Drainage (SAGD) and hot water injection (Teodoriu et al. 2007; Alajmi et al., 2009).

Many authors in both laboratory experiments and numerical simulation have shown that the oil viscosity and mobility ratio can be reduced by hot water injection, ultimately resulting in improved oil recovery (Teodoriu et al., 2007; Taber, 1998; Milton et al., 2003; Prats, 1982; Goodyear et al., 1996; Bousaid, 1991; Jabbour et al., 1996; Okasha et al., 1998; Alajmi et al., 2009). Martin et al. (1968) reported a case study that the hot water flooding yield oil recovery increasing for a pilot test in the Loco field in southern Oklahoma. In other case studies, Pederson and Sitorus, (2001), Wang and Wang (2008), and Chen et al., (2010) indicated that thermal water flooding is superior to conventional water flooding, and can improve oil recovery.

In the case of the Moerkapelle field, operations were stopped because the viscosity of the oil in the reservoir was so high and the reservoir is relatively small such that standard EOR approaches available at the time did not help to produce enough of the available oil. For this reason, the field was abandoned in1986. Below of this stranded field at a depth between 2 and 3 km, there is a sedimentary aquifer (geothermal reservoir) with a temperature of approximately 70 °C to 100 °C, which can be utilized for enhanced thermal heavy oil recovery by providing hot water (EBN, 2013; Ziabakhsh-Ganji et al., 2016, 2018).

As shown by Ziabakhsh-Ganji et al. (2018) the produced oil (in synergy of geothermal and oil recovery) could make the overall project economically feasible or at least decreases the required subsidy: the hot water makes oil production possible and the co-produced oil could reduce the geothermal business case of subsidies up to 50 %. In this paper, further investigations have been conducted to evaluate the synergy potential of the combined energy production from a geothermal reservoir and the heterogeneous heavy

oil reservoir. Moreover, in the oil reservoir model we have employed the numerical simulations of horizontal wellbores taking Bottom Hole Pressure (BHP) constraints into account. To perform such a study, the fluvial reservoir architecture has been considered for the heavy oil reservoir.

In the fluvial reservoir (as a heterogeneous reservoir), the connectivity is via a network of permeable fluvial channel sandstone bodies embedded in non-permeable floodplain mudstone (Willems et al., 2017). The effect of the fluvial reservoir architecture on the recovery of hydrocarbons has been studied extensively (e.g., Jones et al.,1995; Larue & Friedmann, 2005; Larue & Hovadik, 2006, 2008; Pranter et al., 2007; De Jager et al., 2009). To a much more limited extent, this topic is addressed for geothermal energy production (e.g. Hamm & Lopez, 2012; Crooijmans et al., 2016; Willems et al., 2017, Babaei & Nick, 2019), for CO_2 sequestration (e.g. Issautier et al., 2014) and combined CO_2 storage and geothermal energy production (Salimi et al., 2012; Nick et al., 2015). The geometry and distribution of the reservoir bodies control the reservoir connectivity, which is the ratio of the volume of the largest connected reservoir body over the sum of the volume of all reservoir bodies (Crooijmans et al., 2016). The connectivity is closely linked to the Net to Gross ratio (N/G), which is the net reservoir volume versus the total volume (Hovadik & Larue, 2007). Larue and Hovadik (2008) studied the effect of N/G and connectivity, as a measure of reservoir heterogeneity, on oil recovery in a vertical doublet system. For reservoirs with a connectivity above 95 %, they found that geological parameters such as sinuosity and width/thickness ratio of the geobodies and the orientation of the wells compared to the geobodies have a relatively small effect on recovery and water flooding efficiency. There is a small drop in oil recovery when the N/G decreases from 50 % to 20 %. Below 20 % N/G the oil recovery drops drastically from 80 % to roughly 25 % (Larue & Hovadik, 2008).

As mentioned by Ellison and Clayton (1995), reservoir heterogeneity can be a factor to influence the EOR technique performance efficiency in the oil displacement. They used reservoir simulation tools to understand the performance of thermal EOR in a heterogeneous reservoir. They concluded that the steam flood path is strongly affected by reservoir heterogeneity. Gharbi et al. (1997) showed that the degree of heterogeneity and the structure of the reservoir have a significant effect on the efficiency of EOR processes with horizontal and vertical wells. They performed a sensitivity analysis of the EOR by variation of the horizontal well length and the ratio of horizontal to vertical permeability. Alajmi et al. (2014) studied the hot water flood performance in recovering heavy oil using a single horizontal doublet in a heterogeneous reservoir created by a random selection (sample) from a field (population) of infinite extent with the exact and desired Dykstra–Parsons coefficient and correlation lengths. They illustrated that the combination of high permeability variation and high correlation length significantly reduces the displacement performance of horizontal or multilateral wells.

While simulation studies of hot water production from a geothermal source, from both geothermal aquifers and abandoned deep hydrocarbon reservoirs (Crooijmans et al., 2016; Willems et al., 2017a;

Mottaghy et al., 2011; Sanner et al., 2011; Poulsen et al., 2015; Pujol et al., 2015; Tureyen et al., 2015; Daniilidis et al., 2017a; Salimzadeh et al., 2018; Macenić & Kurevija, 2018, Willems & Nick, 2019) and heavy oil are individually well studied, investigations combining the geothermal energy sources and heavy oil reservoirs are still limited. Although a few studies exist for such a combination (Wys et al., 1991; Junrong et al., 2015; Ziabakhsh-Ganji et al. 2018), the integration of geothermal hot water production with EOR from a heavy oil reservoir with a horizontal well doublet has – to our knowledge - not yet been reported.

In this study, the feasibility of generating energy from geothermal resources, both for thermal EOR from a fluvial heavy oil reservoir and for heating purposes is addressed through a numerical study. Connectivity in the fluvial reservoir system and also the effect of Net to Gross ratio (N/G) on Net Present Value (NPV) have been considered. Moreover, the sensitivity analyses of the system corresponding to several parameters, such as horizontal lateral wellbore distance and length of well are explored in order to assess and develop new strategies for integration of geothermal energy with heavy oil production from a fluvial oil reservoir. For this purpose, we have improved our previous model (Ziabakhsh-Ganji et al., 2018) to analyse the effect of these parameters and also how they could control the ultimate heavy oil recovery and the geothermal energy consumption.

2. Methodology

The West Netherlands Basin (WNB) is an example of an area with fluvial geological structures where the exploited reservoirs are usually a porous sandstone from the Lower Cretaceous Nieuwekerk formation (DeVault & Jeremiah, 2002; Van Heekeren & Bakema, 2015). The Moerkapelle oil field, located about 15 km northeast of the city of Delft, is a heavy oil field in the lower Cretaceous Delft Sandstone at a depth of about 800-1000 meters. Below this stranded field at depth between 2 and 3 km, there is a hot sedimentary aquifer (geothermal reservoir) with y a temperature of approximately 70 °C to 100 °C, which can be utilized for enhanced thermal heavy oil recovery (Ziabakhsh-Ganji et al., 2018). The heterogeneity in sediment bodies can be a result of both autogenic as well as allogenic controls (Hajek et al., 2010; Flood & Hampson, 2015) which make it difficult to identify laterally persistent trends on well logs. These types of geological structures are referred to as fluvial architecture which are composed of impermeable floodplain fines and permeable sandstone bodies (Willems et al., 2017). This heterogeneity is a major source of complexity for modelling of the geological fluvial structures.

2.1. Model set up

Analogous to our previous study, (Ziabakhsh-Ganji et al., 2018) the simulation study shown in Figure 1 consists of two domains: 1) a geothermal well doublet (single phase flow model) and 2) a heavy oil (two-phase flow model) reservoir. For the geothermal model (Domain 1 in Figure 1), a three-

dimensional (3D) finite element method was implemented in COMSOL Multiphysics to simulate fluid flow and heat transfer processes in Geothermal Doublets (GeoD), which consist of a hot water production well and a cold water (re-)injection well. Three layers (each with 50 m thickness) are simulated in Domain 1: Overburden, geothermal aquifer and underburden. The model size is 2000 m × 1000 m × 150 m (similar to Figure 2b shown in Willems et al. (2017c)). An initial geothermal reservoir temperature of 100 ˚C and a re-injection temperature of 37 ˚C are considered, corresponding to the initial temperature of the oil reservoir. The production and injection well spacing is 1 km, discharge and injection rate are identical and remain constant over time. The two outer boundaries at the short edge are assigned a constant pressure, the others are no flow boundaries. All other reservoir parameters (Table 1) and the heat transfer process (Appendix 1) are the same as those reported by Ziabakhsh-Ganji et al. (2018).

For the oil reservoir model (Domain 2 in Figure 1), a non-isothermal two-phase flow model developed in ECLIPSE 300 including facies heterogeneity is utilized to investigate the energy consumption for thermal EOR. The size of the oil reservoir model is 500×500 m^2 and 30 m in thickness that includes 1.1205×10^6 m^3 of crude oil as original oil in place (OOIP). The model consists of a 50,000 (100×100×5) grid and includes two horizontal wells (a hot water injector and an oil producer) that lie in the third layer of the model. The energy balance equation for this model takes the following form

$$\frac{\partial}{\partial t}\left[\emptyset \sum_{i=o,w}\left(S_i\left(\rho_i C_{p,i} T - P_i\right)\right) + (1-\emptyset)\rho_r C_{pr} T\right] = -\nabla.\sum_{i=o,w}\left(\rho_i C_{p,i}\boldsymbol{u}_i\right)T + \nabla.\left(\boldsymbol{\lambda_2}\nabla T\right) \quad (1)$$

where the subscripts *o*, *w* and *r* refer to the oil, the water, and the solid phase (rock) respectively. $\emptyset$ is the oil reservoir porosity and $\boldsymbol{\lambda_2}$ is the bulk thermal conductivity [W/(mK)], ρ [kg/m^3] and *S* [-] are the density and saturation of each phase respectively. In Eq. (1), it is implicitly assumed that local equilibrium is established (Ziabakhsh-Ganji & Kooi, 2014). Mass conservation is represented by

$$\frac{\partial}{\partial t}\left[\emptyset_2 \sum_{i=o,w}\left(S_i\rho_i\right)\right] + \nabla.\sum_{i=o,w}\left(\rho_i\boldsymbol{u}_i\right) - Q^* = 0 \quad (2)$$

where the specific volumetric velocity $\boldsymbol{u}_i$ is given by Darcy's law,

$$\boldsymbol{u}_i = \frac{-k k_{ri}}{\mu_i}\nabla P_i \quad (3)$$

where μ_i is the viscosity of each phase (oil/water) and Q^* is source/sink respectively.

Here the relative permeability data (k_{ri}), that are derived from laboratory measurements of capillary pressure ($P_c = 0.2425[S_w - 0.0603]^{-1.4141}$) on core plugs (extracted from wells) flooding tests (Figure 2) and the Brook and Corey correlation, is utilized based on the following parameters: $S_{wi} = 0.17$, $S_{orw} = 0.05$, $S_{org} = 0.1$, $S_{gc} = 0, k_{roiw} = 0.4$, $k_{rwro} = 0.4$, $k_{rwro} = 0.1$, $k_{rgro} = 0.2$ and $S_{wir} = 0.17$. The capillary pressure is also included in the model in order to be more realistic in comparison with Moerkapelle oil field. The oil viscosity and oil density are 850 cp and 15 °API at the initial reservoir condition, respectively (EBN, 2013). The correlation for prediction of the heavy oil viscosity, as a function of temperature and the oil API, is taken from Ziabakhsh-Ganji et al., (2018) which was modelled by the Artificial Neural Network technique.

While the permeability (k in Eq. (3)) of the reservoir varies, thermal properties including thermal conductivity and heat capacity of rock are assumed to be homogeneous, but different for the cap and the base rocks. Rock thermal properties used are the same as those employed by Ziabakhsh-Ganji et al. (2018). For modelling of the depositional pattern, the process-based facies modelling software FLUMY has been employed to generate 150 realisations (depositional models) of a 500 m × 500 m × 30 m oil reservoir with a resolution of 5 m × 5 m × 6 m. Similar to Crooijmans et al., (2016), the resulting realisations comprise seven types of geobodies which are pointbars, sand plugs, channel lag, crevasse splays, levees, overbank floodplain fines and mud plugs. However, the avulsion frequency, flood frequency, paleo-channel width and depth, maximum floodplain deposit thickness and topography of the floodplain are the main factors that can control the sedimentological processes (Crooijmans et al., 2016). The paleo-channel information such as width and depth, extracted from well core data interpretations of the (DeVault & Jeremiah, 2002), are assumed to be 40 m and 4 m, respectively. Since the permeability is non-uniform throughout the reservoir, N/G ranging from 10 to 70 % were used. The other parameter values used in the modelling are listed in Table 2.

MATLAB was used as an interface to translate the FLUMY output (reservoir realisations) into ECLIPSE 300 input data. For this purpose, and to simplify the model, the 7 types of geobodies are grouped into either sand or shale. Channel lag, point bar and sand plug are considered as sand group (reservoir) and the others as shale group (non-reservoir) respectively. These groups are utilized to calculate N/G of the realisations (Figure 3). Since the grain size of each geobody is different, the permeability of the sand is considered heterogeneous which strongly depends on paleo flow speed (Figure 3), and the proximity to the channel axis and river bends. Consequently, the permeability of channel lags, point-bars and sand plugs as those captured by using of the sandstone permeability distribution from the core measurements (TNO, 1977) varies across sandstone bodies (Willis & Tang, 2010). In order to generate a heterogeneous reservoir within the sand group we have used a beta distribution correlation function (Crooijmans et al., 2016). The distribution characteristics including: mean, standard deviation, skew and kurtosis are equal

to 0.28, 0.075, 0.35 and 2.3, respectively, as used by Crooijmans et al., (2016). Based on petrophysical data of well MKP-11 the porosity-permeability relationship can be described by

$$k = 0.0663e^{29.507\emptyset} \tag{4}$$

where k is the permeability [mD] and ϕ is the porosity [–]. The effect of heterogeneity in the thermal rock properties on heat transfer in the geothermal reservoir is insignificant compared to the heterogeneity in the flow properties (Crooijmans et al., 2016). Therefore, thermal rock properties are considered homogeneous and isotropic. The porosity and permeability of the shale group are also assumed to be homogeneous and isotropic with values of 0.1 and 5 mD, respectively (Crooijmans et al., 2016). The Bottom Hole Pressure (BHP) is considered to be 11.51 MPa (1669 Psi) which is selected based on Dutch Ministry of Economic Affairs permission for the injection well at oil reservoir depth of 800 m. It is assumed that water is in the liquid phase and can be supplied continuously without well integrity problems in the case of unconsolidated sandstone during the entire injection period. The oil producer is controlled with the bottomhole pressure of 0.7 MPa (100 Psi) and the target rate is the same as the injection rate value (Ziabakhsh-Ganji et al., 2018).

It is noteworthy to mention that, in this study, we assumed that the geothermal domain is homogenous while the oil reservoir domain is heterogeneous. This is useful since it renders the impacts of N/G on the synergy of geothermal energy and heavy oil production clearly visible. We further assumed that the hot water with a temperature of 100 °C producing from geothermal doublet does not inject in the oil reservoir (which has an initial temperature of 37 °C) directly. In other words, therefore, the geothermal energy can provide the required heat for the heating up the water for the TEOR.

2.2. Equivalent Permeability on realisation scale and in horizontal well pairs

In steady-state, a 0.31 MPa (45 Psi) psi pressure difference (∇P) was consecutively applied in three dimensions between opposite realisation boundaries using Eclipse 100 simulation software (e.g. Willems et al., 2017). To determine the fluid pressure field, the single-phase steady-state continuity equation was solved with constant viscosity (μ) using

$$\nabla.\left(\frac{K_{facies}}{\mu}\nabla P\right) = 0 \tag{5}$$

In this balance, K_{facies} is the permeability field which is assigned to the grid blocks in each realisation and μ is the water viscosity (0,001 Pa.s). The detailed modelling procedure follows the approach by Saeid et al., (2014, 2015). Subsequently, by employing the fluid flux (q) of horizontal wells on which

the pressure difference is applied, the equivalent permeability K_{eq} can be determined using Eq. (6) (e.g., Joshi, 1991)

$$K_{eq} = \frac{q_H \mu}{h \Delta P}\left[\ln\left(\frac{A + \sqrt{A^2 - \left({}^{L}/_{2}\right)^2}}{{}^{L}/_{2}}\right) + {}^{h}/_{L} \ln\left(\frac{h}{2r_w}\right)\right] \quad (6)$$

where h and L are the reservoir thickness and horizontal well length respectively. r_w is the wellbore radius and A is the drainage area relation, which can be calculated through

$$A = \frac{L}{2}\sqrt{\left(\frac{1}{2} + \sqrt{\frac{1}{4} + \left(\frac{2r_{eh}}{L}\right)^4}\right)} \quad (7)$$

In Eq. (7), r_{eh} is the geometric factor that is related to the drainage area shape (Joshi, 1991). The derived equivalent permeability was related to the N/G of the realisation in the analysis of the results. The simulations yielded a required pressure difference between wells for a 1000 m^3/day production rate. This pressure difference was used to determine equivalent permeability between wells using Eq. (3) (Willems et al., 2017). The N/G was the main parameter in our analyses and varied between 15 % to 70 % in the realisations. The equivalent permeability analysis between the well pairs was calculated for different horizontal well length and wellbore spacing.

2.3. Model validation

In this section, the numerical uncertainties for model convergence evaluation are studied. For this purpose, the model was executed with progressively finer grid sizes in order to minimise the numerical uncertainties in computational simulations such as numerical dissipation and discretization errors (Nick et al., 2009). The size of the grid cells is gradually decreased until there is no significant difference in the numerical results between two successive mesh densities (Saeid et al., 2015; Ziabakhsh-Ganji et al., 2018).

For the geothermal reservoir Domain (1) we have followed the approach in our earlier study (Ziabakhsh-Ganji et al., 2018). For the oil reservoir model (Domain 2) our results indicate that a grid cell with an average grid size of 5 m × 5 m × 6 m (100, 100 grid cells in *x*, *y* and 5 in *z* directions respectively) is sufficient (Figure 4).

2.4. Pump energy

The energy required for water injection in the reservoirs is the main source of energy consumption in both geothermal energy production and TEOR. The energy required for the pump, which generates a pressure difference between the injection and the production wells, can be calculated through Eq. (8)

$$E_{pump}^{Geo} = \frac{\sum_{i=1}^{n} Q_R^{Geo} \Delta t_i \left(P_{inj} - P_{prod}\right)_{geothermal}}{\epsilon} \tag{8}$$

where Q_R^{Geo} is the discharge rate of the geothermal reservoir Domain (1), which is identical for both injection and production wells.

Similarly, for the oil reservoir Domain (2) the energy required for the pump can be obtained through

$$E_{pump}^{oil} = \frac{\sum_{i=1}^{n} Q_R^{Oil} \Delta t_i \left(P_{inj} - P_{prod}\right)_{oil}}{\epsilon} \tag{9}$$

In Eqs. (8) and (9), ϵ is the efficiency of the pumps, which is assumed to be 1.

3. Results

The results of our simulations are subdivided into two subsections: one for the geothermal reservoir and the other one for the heavy oil reservoir. The main focus of these studies is on the N/G investigation in the heavy oil reservoir domain.

3.1. Geothermal system (Domain 1)

For the geothermal reservoir (Domain 1), the transient water temperature at the production well is calculated for several injection rates (Figure 5). As shown in Figure 5a, there is a significant reduction in the production temperature after 20 years when the discharge increases from 1680 m^3/day to 6000 m^3/day (Willems, 2017b; Ziabakhsh-Ganji et al., 2018). By contrast, the results show that for higher injection rate values the produced energy is enhanced (Figure 5b), which is in accordance with the findings of Ziabakhsh-Ganji et al. (2018). When the thermal front (cold water) reaches the production well such that the temperature breakthrough occurs the temperature of the pumped up from the production well gradually decreases from the initial geothermal reservoir temperature until it eventually reaches the injection temperature, if injection is not stopped. Figure 5a indicates that higher discharge rates result in sharper breakthrough curves. An explanation for this behaviour is that the velocity of the injected water in the porous pathway increases as the injection rate increases. Therefore, the quantity of thermal energy transferred from the surrounding rock to the injected water decreases. As shown in Figure 5a, it is noticeable that the system is far from steady-state equilibrium even after 150 years.

The reason is that the thermal transfer process between rocks and injection fluid is at unsteady state and quite slow. This is in accordance with the findings of Saeid et al., (2015) and Vik et al., (2018).

In order to adequately assess the net energy production of a geothermal doublet, the required energy for pumping should be taken into account and subtracted from the total energy production. The total energy production from a geothermal doublet can be calculated through $\Delta\dot{E}_\iota = \dot{m}_\iota c_p \Delta T_i$, where $\Delta\dot{E}_\iota$ (J/year) is the annual thermal energy extracted in the i^{th} year, $\dot{m}_\iota$ (*kg/year*) is the total mass production of hot water in the i^{th} year, c_p (*J/kg K*) is the specific heat of the circulating fluid and ΔT_i (*K*) is the temperature difference between the produced and injected fluid in the i^{th} year. The total net produced energy for *n* years of production can then be obtained as the summation of the energy provided on overall *n* years minus the pump energy that is required to induce a pressure difference between the injection and the production wells: $E_n^{Geo} = E_{prod}^{Geo} - E_{pump}^{Geo}$ (Willems et al., 2017b).

Figures 5c and 5d show how the pump performance changes with time. By increasing the discharge rate, the pressure difference is also increased. In fact, by injecting cold water in the reservoir the injection pressure increases because of higher viscosity of the cold water compared to that of hot water in the reservoir. As a result, the cumulative energy utilized for the pumps increases. The increase, however, is quite small in comparison with the increased cumulative produced energy with increasing discharge rate.

3.2. Heavy oil reservoir (Domain 2)

3.2.1. Effect of the N/G

Fluvial reservoir geology leads to a complex behaviour in terms of flow and heat transfer and mass transport, which requires the integration of heterogeneity in our simulations. In order to understand such influences, we consider the impact of N/G on the equivalent permeability by executing several hundred scenarios. Figure 6 shows the equivalent permeability and pressure drops for different horizontal well lengths and wellbore spacing, which is calculated through Eq. (6). The relation of the equivalent permeability K_{eq} with N/G has a contrasting trend compared to the pressure drops: the pressure difference decreases with increasing N/G, while permeability increases. This behaviour clearly indicates a dependence of fluid flow on N/G.

Below N/G of 50 %, pressure drops and equivalent permeability show an exponential dependence on N/G, while above 50 % N/G, they have a linear relation with N/G, meaning that the effect of N/G on the pressure drops is more important at low values. It is notable that the equivalent permeability increases gently in comparison with the pressure drop whenever the N/G increases.

In order to understand the effect of horizontal well length and spacing on the equivalent permeability several simulations were carried out by varying the length between 200 m to 400 m, and the spacing between 100 m to 200 m. Figures 6c and 6d illustrate the contribution of the well length and well spacing on the equivalent permeability calculation. By increasing the length of the horizontal wells, the equivalent permeability is enhanced. By contrast, there is a reduction in the equivalent permeability of the system when the wellbore spacing increases from 100 m to 200 m. This effect is more pronounced for lower N/G values.

To derive the oil recovery factor (RF), it makes sense to look at the pressure drop and effective permeability for different N/G. Below 50 % N/G, the pressure drop to N/G relation has a large standard deviation. Due to this uncertainty in the pressure drop, more clustering regions are required for the N/G lower than 50 % to determine a stable average. Figure 7 shows 6 clustering ranges: 1) 15 – 20 %, 2) 20 – 25 %, 3) 25 – 30 %, 4) 30 – 40 %, 5) 40 – 50 % and 6) greater than 50 %. The effect of these cluster values on the estimation of the oil Recovery Factor (RF) and total cumulative oil production (TOP) in the oil reservoir domain is illustrated in Figure 8. The resulting average oil recovery factors were calculated for each cluster and are shown in red solid lines in figures 8a to 8f. As shown in figures 8g and 8h, the resulting all realisations and the average RF range from 2 % to 15 % increase with the enhancing of the N/G. This is because for the higher N/G reservoirs the injection rates are higher than those of reservoirs with lower N/G values. This means that higher N/G causes earlier temperature breakthrough (and hence increasing demand) for hot water flooding in the reservoir resulting in the oil recovery enhancement. By contrast, the simulation results show that the oil recovery is rather insensitive for N/G values > 30 %.

Because results for the clusters with lower N/G values on RF are similar, we defined new clusters as follows: a) 15 – 30 % b) 30 – 50 % and c) 50 – 70 % of N/G. For each cluster one N/G value is considered as a representative value of the whole cluster in which N/G of 28.3 %, 42.6 % and 61.3 % have been allocated for group a, b and c, respectively.

In order to explore the effect of lower N/G on RF in more detail we have extended the model calculations to 40 years (Figure 9). As illustrated in figure 9a, for the low value of N/G (28.3 %) the ΔRF is less than 5 % after 40 years. For higher values of N/G the amount of ΔRF is enhanced up to 12 %. A similar increase is observed for ΔTOP (Figure 9b). The ΔRF and ΔTOP indicate the oil recovery factor (RF) and total cumulative oil production (TOP) difference between conventional water flooding (the injected water temperature similar to that of the oil reservoir) and hot water flooding. Moreover, the hot water injection amounts (Figure 9c) show a similar relation with N/G. However, a considerable difference between the amount of cold water and hot water flooding is exhibited in Figure 9d. Forasmuch as a high value of the N/G favours high RF (as shown in Figure 9a), large amounts of hot water are needed to enhance RF for high values of N/G (Figure 9d). For producing about 30 m^3/day oil, about 7000 m^3/day

of hot water is needed to inject in the reservoir. For the overall project economics, the extra produced oil should exceed the cost for the provision of the hot water (Figures 9d and 9f). Through the calculation of the Net Present Value (NPV) in section 4, we try to determine the economic feasibility of the current project.

For the economic feasibility of the TEOR the Temperature Breakthrough Time (TBT) plays a crucial role. At high values of N/G the TBT occurs earlier than for lower N/G. In other words, the onset of TBT is very sensitive to the N/G (Figure 9e).

3.2.2. Effect of wellbore distances, length and BHP

Operational conditions such as wellbore spacing, wellbore length and BHP, which are human control parameters, play essential roles in thermal EOR. In order to understand the impact of these parameters on the produced oil, several scenarios have been considered such for three different values of a) well spacing (D) of 100 m, 150 m and 200 m; b) horizontal well length (L) of 200 m, 300 m and 400 m; and c) BHP of 10.34 MPa (1500 Psi), 11.51 MPa (1669 Psi) and 13.8 MPa (2000 Psi).

Figure 10 shows the effect of horizontal wellbore distances, lengths and the BHP on ΔTOP and ΔInj rates. As illustrated in figure 10, oil recovery is increased by increasing wellbore length and BHP, while the wellbore spacing increase has an adverse effect on ΔTOP. In figures 10a and 10b, scenarios with increased wellbore distance decrease the ΔTOP and, hence, ΔInj rates. Longer distances between injection and production wells lead to a delay in the TBT. For instance, with a distance of 200 m (even after 40 years of hot water injection) no enhanced oil recovery has started. The possible explanation for this effect is the extended time it takes for the heat plume to reach the production well when the well spacing is too large, such that the oil viscosity reduction initially just happens near the injector.

As shown in Figure 10c to 10f, increasing the well length and BHP leads to a higher ΔTOP and ΔInj rates. Furthermore, TBT changes are slightly sensitive to increasing wellbore length. However, at high values of BHP the TBT occurs at an earlier time in comparison with a lower BHP, which leads to a more significant improvement in the oil recovery factor. This means that while TBT is sensitive to increasing of the wellbore spacing and BHP, it is almost unaffected by the wellbore length variations.

3.2.3. Effect of oil viscosity

In the thermal EOR method, the oil viscosity, which is dependent on temperature, has a significant influence on the oil recovery. In order to further investigate the effect of oil viscosity in the hot water injection process, several additional simulation runs were conducted to cover four different oil viscosity types, as listed in Table 3. Figure 11 shows the results of these runs. The figure compares the total oil

production and injection rates for the different oil viscosity types versus time of hot water injection period up to 40 years.

As shown in figure 11, the Coalinga oil reservoir outperforms all others, while the Cymric oil reservoir underperforms most noticeably compared to the others. Figure 11b displays that the results of ΔTOP for Coalinga, KernRiver and Moerkapelle reservoirs are similar for the first 30 years and hardly show any difference after 40 years. Furthermore, from figures 11c and 11d, it appears there is a direct relationship between oil viscosity and amount of hot water injection. The improvement of hot water injection is more pronounced in reservoirs with lighter oil viscosity.

Lighter viscosity oil (e.g. Coalinga oil) results in better oil sweep in the reservoir within a shorter time despite an earlier water breakthrough. This is because an increase in the oil viscosity (e.g. Cymric oil) leads to an increased TBT, which implies a slower propagation of heat towards the oil production well.

3.2.4. Consumed energy for the thermal oil recovery

The role of hot water in EOR is energy provision to raise the oil temperature to a level that allows flow and production. This energy provision needs to be accounted for in the total energy balance of the exploited system. The difference in cumulative consumed energy for heavy oil production between conventional water flooding (the injected water temperature similar to that of the oil reservoir) and hot water flooding, ΔE_n, and its dependence on the various parameters investigated here is shown in Fig. 12. The cumulative consumed energy (E_n) is defined here as the difference between the total energy injected into and the energy produced from the oil reservoir and the required energy for pumping of the hot water:

$$E_n = E_{inj} - E_{Prod}^{oil} + E_{pump}^{oil} \tag{10}$$

where E_{Prod}^{oil} is the produced energy from oil reservoir and E_{inj} is the cumulative energy with respect to the initial oil reservoir temperature, calculated through

$$E_{inj} = \sum_{i=1}^{n} Q_i \Delta t \rho_f Cp_f \left(T_{inj} - T_s\right) \tag{11}$$

$$E_{Prod}^{oil} = \sum_{i=1}^{n} Q_{w,prod} \Delta t \rho_f Cp_f \left(T_{prod} - T_s\right) \tag{12}$$

where Δt is the time step [day], n is the number of time steps, Q_i is the hot water injection rate, T_{inj} is the injection temperature, $Q_{w,prod}$ is the hot water production rate from the oil production well and T_{prod} is the production temperature (see Figure 9e). Similar to Ziabakhsh-Ganji et al. (2018) it is

assumed that at the beginning of the hot water flooding, surface water with a temperature of 10 °C (T_s) and with identical thermal properties of the formation water can be utilised until enough water for reinjection is produced from the oil reservoir.

As shown in Figure 12, the consumed energy increases with N/G up to about 500 GWh after 40 years (Figure 12a). Given that high permeable zones allow large quantities of hot water to flow, the consumed total energy is increased for high N/G. the same effect is predicted for a short distance (100 m) and longer length of wellbores (400m) and higher values of the BHP (2000 Psi). However, due to the higher pressure difference between injection and production wells for higher BHP the required energy for hot water pumping is increased (Figure 12b). The difference in total consumed energy for the various parameters compared to the total oil produced ΔTOP is shown in Figures 12e to 12h. For increasing N/G and for greater wellbore lengths, generally more oil can be produced, while the effect of the BHP seems to be negligible, at least within the pressure range investigated here. The effect of wellbore spacing looks a bit more complex. At point A in Figure 12g the total oil production (ΔTOP) for 100 m and 150 m wellbore distance are identical at $\Delta E_n = 214.8$ GWh. However, this value is reached at different times after hot water injection. For 100 m wellbore distance, the time required for reaching point (A) is about 22 years, while for 150 m it is reached 36.5 years after the onset of the hot water injection. As a result, at a given cumulative energy consumption ($\Delta E_n = 214.8$ GWh) the total oil production ($\Delta TOP = 9.75 \times 10^4$ m^3) for 100 m wellbore spacing is equivalent to that for 150 m. Such behaviour is not predicted for 200 m wellbore spacing.

The effect of viscosity investigating the same parameters as above is shown in Figure 13 for different oil types. There is a strong effect of viscosity on the difference in energy consumed for production. The energy required to produce oil for Coalinga, KernRiver and Moerkapelle reservoirs is about 2 times larger than that of the Cymric (the oil with the highest viscosity) at the end of 40 years. Only a relatively small difference in results for Coalinga, KernRiver and Moerkapelle was found. Coalinga, KernRiver and Moerkapelle reservoirs need about the same energy for TOP (just over different time periods), while for Cymric more energy is required in order to reach the same TOP. For instance, at a given cumulative energy consumption ($\Delta E_n = 200$ GWh) the total oil production (ΔTOP) for Cymric is 8×10^4 m^3 and for the others, it is about 9.5×10^4 m^3 (points A and B in figure 13b). The time required to reach these points is different for the different oil types: 15.5, 18.7, 21.14 and 37.8 years for Coalinga, KernRiver, Moerkapelle and Cymric reservoirs, respectively.

4. Discussion

4.1. Geothermal doublets

The discharge from a geothermal doublet has been used to provide the heat required for EOR in this study. While N/G in fluvial reservoirs plays a significant role in our calculations, here, we assume that

the geothermal reservoir domain is homogenous with an initial temperature of 100 °C, providing the required energy for heavy oil production. The influence of the N/G on life time, heat recovery and pumping energy of a geothermal doublet have been described in the study by Crooijmans et al. (2016) comprehensively.

The current study addresses cumulative energy production (including the required energy for cold water pumping) from a geothermal doublet with various injection rates (Figure 5). The results show that the cumulative energy harvesting and pump energy over 40 years from a geothermal doublet for injection rate 6000 (m^3/day) are 6189 GWh and 43.9 GWh respectively. In fact, the comparison of the two plots (Figures 5b and 5d) indicates that less than 1 % of produced geothermal energy is consumed by the energy required for the pump. Thus, based on the results shown in figures 5b and 5d, the geothermal aquifer can serve as a long-term source of hot water injection into the oil reservoir in order to thermally enhance the heavy oil recovery.

4.2. Effect of N/G

This study illustrates that higher N/G causes early water breakthrough for hot water flooding (and hence TBT) in the reservoir resulting in the oil recovery enhancement. However, low values of the N/G have almost a negligible influence on the oil recovery. Therefore, it seems that the TEOR method is not applicable in fluvial reservoirs with low values of N/G.

As is shown in the results, heterogeneity has a significant effect on how heavy oil is displaced by the injected hot water. A low value of the N/G has a very minimal influence on the heat distribution in the reservoir. This is due to the fact that the injected fluid tends to follow the high permeability zone and therefore heat is propagated in these zones causing to lower oil viscosity where it is displaced (Alajmi et al., 2009). More specifically, the N/G has a strong relationship with the connectivity of the pores (permeability) in the reservoir rocks.

Based on the obtained equivalent permeability for the base case scenario shown in Figure 7, the equivalent permeability can be described as a function of N/G such that

$$K_{eq} = \begin{cases} 10.0533e^{0.0416\times N/G} & 15 < N/G < 50 \\ 0.0957 N/G^{1.7356} & 50 \leq N/G \end{cases} \quad (13)$$

In order to show the dependency of the equivalent permeability on the N/G this equation is only tested for realisation with N/G between 15 to 70 % and wellbore length and wellbore distance of 300 m and 100 m, respectively. However, the impact of other parameters such as wellbore length, wellbore distance and reservoir dimensions (e.g., thickness) can be included in this relation as well. As shown in figure 8, a higher value of N/G leads to a higher value of equivalent permeability. This means that increasing of

the reservoir permeability leads to enhanced production of oil. However, the opposite behaviour is observed for increasing permeability in our previous study (Ziabakhsh-Ganji et al., 2018), in which ΔTOP slightly decreases for increasing permeabilities within the range investigated. The reason for different behaviour in this study appears in the model set up the assumption.

In the study of Ziabakhsh-Ganji et al., (2018) there was no restrictions defined for the injection well. In this work, however, we considered a BHP constraint (based on national regulations) for the water injection wellbore to avoid inducing fractures in the reservoir. Therefore, the injection rate for hot water into the oil reservoir domain is limited by taking the BHP restriction into account, and the injection rate changes in time as the total mobility changes by advancing the hot water plume.

4.3. Effect of BHP well length and wellbore distances

The BHP, well length and wellbore distances as human control parameters play an important role in thermal EOR projects. A guide value for a liquid pressure limit acceptable to all applications at the top of the reservoir is a pressure gradient of 0.0135 MPa / depth (m), which is based on the expected lower limit of fracture propagation pressure at that level. However, there is a correction for the influence of thermal effects on fracture propagation and a safety margin that is excluded in this relation. The Maximum BHP (MBHP) based on well test analysis is suggested as $MBHP = TVD \times (0.135 - Gr_{Pr})$, where TVD is the true vertical depth and $\mathrm{Gr_{Pr}}$ is hydraulic gradient of the local water injection, which is 0.0105 MPa/m for the Moerkapelle reservoir, resulting in a minimum BHP of 11.5 MPa (~1669 Psi) at a depth of 800 m.

As shown in figure 12 and Eq. 9, higher BHP leads to higher consumed total energy for both pumping and hot water injection. This higher energy consumption, however, is compensated by the extra produced oil.

Among all human control parameters, wellbore spacing and length have the strongest effect, more than reservoir parameters (such as porosity and permeability) on the distribution of the temperature plume and the resulting oil production, i.e., the improved ΔTOP and reduced ΔE_n. Our results show that 100 m well spacing gives an optimum value of oil recovery for horizontal wells, which is in accordance with the results of Cheung et al. (2013), Zhao et al., (2014) and Verney, (2015), who defined a profitable range of 80m to 250m. Longer distances are also theoretically possible for EOR, covering a higher amount of original oil in place (OOIP), but they require more extended injection periods, which uses much more energy.

Our results show that although a larger length of the horizontal section of the wellbores leads to favourable oil recovery, it has no effect on the TBT, however, as the wellbore length increases the amount of injected hot water dramatically.

Furthermore, in this study, we suppose that the horizontal well doublet is oriented perpendicular to the paleo flow trend of the fluvial system. The effect of changing the orientation of the horizontal wellbore sections with respect to the reservoir rocks may be significant and needs further investigation, but it was not within the scope of this study.

4.4. The role of geothermal doublets on the required energy of the oil reservoir

The results presented in the previous sections comprise our understanding of how oil production from stranded oil fields (fields abandoned when field development was considered not to be profitable), especially those with heavy oil, can add value to a geothermal project, when the hot water required for thermal EOR comes from a geothermal reservoir and coproduction of oil and geothermal energy is considered.

In our calculations for the geothermal reservoir, we assumed a discharge rate of 3600 m^3/day, a relatively conservative value exceeded by all currently operating geothermal doublets in the Netherlands. As shown in Figure 14, only a fraction of the energy provided is required for the improved oil production, assuming one doublet of oil wells. The figure shows the ratio of the total consumed energy per total energy provided by the GeoD ($E_n/E_{geothermal}$). However, what is not shown here, is how this ratio changes when the discharge rate of GeoD are changed and the energy production from oil the production wells are not taken into account. For example, for consuming less than 10 % of extracted energy from the GeoD, 13.5×10^4 m^3 of oil could be produced, which is about 12% of the OOIP (1.58×10^6 m^3), after 20 years of hot water injection with a temperature of 100°C when N/G is 61.3 %.

As soon as the warm water reaches to production wells, however, the demand for hot water injection is drastically increased leading to a much higher energy demand (that are supplied by GeoDs). Therefore, when the injection rates into the oil reservoir are increased the required geothermal discharge may exceed what can be supplied by one GeoD. Note that as shown in Ziabakhsh-Ganji et al., (2018) the produced water from the oil production well has a high temperature. Therefore, the total energy required for the injection of hot water is not linked directly to the injection rate.

4.5. Feasibility Analysis

For an economic feasibility analysis, we assume a pre-royalty-pre-tax framework. Since, there are no similar projects in the Netherlands, it is still not known how Geothermal-EOR projects (Ziabakhsh-

Ganji et al., 2018) would be taxed. Analogous to the study of Ziabakhsh-Ganji et al., (2018) and Aramburo Velez (2017) the oil price used is 50 USD/STB (~45.5 Euro/STB), heat price 0.012 Euro/kWh (ECN, 2017) and the discount rate is 8%. The Investment and Operational costs (CAPEX and OPEX) and the price of the heat used in the economics of the geothermal project are based on a price per kilowatt (kW) output of heat as reported by ECN (2017). The capex of the wells introduced by van Wees et al. (2010) is considered for calculating the well drilling costs

$$E_{capex\_well} = s\,(0.2Z_r^2 + 700Z_r + 250 \times 10^3) \times 10^{-6} \quad (14)$$

where s is a variable representing the well scaling factor, Z_r is the measured depth (TVD) and costs are calculated in million euros. s was chosen to be 1.72 for the calculations, following Daniilidis et al. (2017b). We also assume that the cost of horizontal well drilling is analogous to that for a vertical well. The other information for calculation of NPV is displayed in Table 4 for both geothermal and EOR projects.

The results show that the synergy between geothermal heat generation and EOR with horizontal wells may compensate for the required subsidy. As shown in figure 15, chances for a viable project requiring no subsidy for the geothermal project are increased for high values of N/G, larger wellbore length and also the lower the viscosity of the oil. The NPV analyses for different N/G show that, at low N/G (e.g., 28.3 %) and high viscous oil (e.g., Cymric) the required subsidy for a single doublet geothermal project is increased, which implies that a synergy project for this type of reservoir is not a viable option (Figure 15a).

Overall, the total energy production is, in all the cases, higher than what would be obtained from a geothermal doublet with a constant production rate. Even in cases where the synergy project may not be interesting from an economic point of view (single doublets); the extra production of energy compared to a geothermal project makes it viable from the enthalpy side (energy point of view).

5. Conclusion

In this work, for assessing the synergy potential of the fluvial heavy oil reservoir and the geothermal production considering different scenarios such as horizontal well, BHP and viscosity two different models have been developed. For this purpose, a finite element non-isothermal flow model for geothermal doublet and a non-isothermal fluvial flow transport modelling for the heterogeneous oil reservoir are utilized to handle the combined heat and multiphase flow simulations.

From the various scenarios (such as N/G, BHP, oil viscosity, horizontal wellbore length and spacing) that are investigated in this study the following conclusions can be drawn:

- Geological heterogeneity, represented here by the varying values of N/G, significantly impacts enhanced oil recovery from a heavy oil reservoir. The oil recovery is more effective in reservoirs with higher N/G.
- The temperature effect on oil recovery takes time. The high temperature profile does not immediately arrive at the producer as the oil viscosity reduction just happens near the injector. Initially, no significant oil saturation alteration in the reservoir and near the producer is observed. As the hot temperature front slowly migrates through the reservoir, oil viscosity is also reduced and eventually reaches the producer, which then leads to increased production rates. Thus, well spacing is of crucial importance for the efficiency and economics of the project.
- The influence of wellbore length and the BHP on the amount of oil recovered is identical. Long wellbore length and high value of the BHP are favourable for EOR as more hot water is injected in the injection wells than for short wellbore lengths and lower values of BHP.
- While large values of the BHP, N/G and wellbore length lead to enhance the oil recovery, increasing the wellbore distance and oil viscosity has an inverse effect on thermal EOR.
- After 40 years of continuous hot water injection, less than 10 % of the energy extracted from a geothermal doublet (with a discharge rate of 3600 m^3/day) is needed to improve the oil recovery factor by 12% in Moerkapelle reservoir, if one well doublet is used for oil production. However, the amount of energy (and hot water injection) required changes significantly with time when TBT is reached in the oil reservoir.
- In a heterogeneous reservoir, the synergy between geothermal and stranded oil fields may compensate the required subsidy for a single doublet geothermal project, which can make the synergy project economically attractive.

Acknowledgment

The authors thank EBN for financial support of the project research of the first author. The authors would further like to thank Dr. M.E. Donselaar for general assistance in the understanding of fluvial reservoir properties.

Nomenclature

$\Delta\dot{E}_t$	annual thermal energy extracted	E_{inj}	Energy injection in oil reservoir domain
$\dot{m}_t$	mass production of hot water	E_n	cumulative energy consumption in oil reservoir
c_p	specific heat	Q_{inj}^w	Water injection rate in oil reservoir domain
ΔT_i	temperature difference between the produced and injected	Q_{pro}^w	Water production rate in oil reservoir domain
P	pressure	T_{init}	initial temperature in oil reservoir domain
$\boldsymbol{u}$	Darcy velocity vector	T_{inj}	injection temperature in oil reservoir domain
K_{eq}	Equivalent permeability	T_{pro}	Production temperature of oil reservoir
k_{ri}	Oil and water relative permeability	T_s	Surface temperature
TVD	True Vertical Depth	NPV	Net Present Value
S_{orw}	Residual oil saturation	S_a	Brine salinity (M)
S_{wir}	Initial water saturation	MWh	Megawatt hour
ΔTOP	Total oil production variable (TOP for elevated Temperature injection – TOP for T_{inj} =37 ºC)	ΔRF	RF at T_{inj} =100 ºC – RF at T_{inj} =37 ºC)
L	Horizontal well length	GWh	Gigawatt hour
D	Distance between injection and production wells in oil reservoir domain	RF	Recovery factor
Gr_{Pr}	Pressure gradient	ϵ	Pump efficiency
N/G	Net to Gross ratio	ρ_f	Density of fluid (oil/water)
TBT	Temperature Breakthrough Time		

References

Alajmi A.F., Gharbi R., Algharaib M., The effect of heterogeneity and well configuration on the performance of hot water flood, Journal of Petroleum Science and Engineering, 122, (2014) 524-533.

Alajmi A.F., Gharbi R., Algharaib M., Investigating the performance of hot water injection in geostatistically generated permeable media, Journal of Petroleum Science and Engineering, 66 (3–4), (2009) 143-155.

Aramburo Velez, D.A., (2017), Synergy between geothermal and stranded oil fields to add value to geothermal projects, MS thesis, Delft University of Technology, Delft, the Netherlands.

Babaei M., & Nick H.M., Performance of low-enthalpy geothermal systems: Interplay of spatially correlated heterogeneity and well-doublet spacings, Applied energy 2019 (in press).

Bousaid I.S., Hot-water and steamflood studies using kern river oil, International Thermal Operations Symposium, Bakersfield, California, vol. 21543, SPE (1991).

Chen T., Zhang Z., Liu Y., Experiment research on the impact of geothermal water temperature on heavy oil recovery factor, Special Oil and Gas Reservoirs, 17(1), (2010), 98-99, 104 (in Chinese).

Cheung K.L.H., SAGD Well Pair Spacing Evaluation with Consideration of Central Processing Facility Constraints, SPE-165397-MS, (2013).

Crooijmans R.A. , Willems, C.J.L., Nick, H.M., Bruhn, D.F., The influence of facies heterogeneity on the doublet performance in low-enthalpy geothermal sedimentary reservoirs, Geothermics, 64, (2016), 209–219.

Daniilidis A., Alpsoy B., Herber R., Impact of technical and economic uncertainties on the economic performance of a deep geothermal heat system, Renewable Energy, 114, (2017a) 805-816

Daniilidis A, Scholten T, Hooghiem J, De Persis C, Herber R. Geochemical implications of production and storage control by coupling a direct-use geothermal system with heat networks. Applied Energy. 204 (2017b), 254-70.

De Jager G., Van Doren J.F.M., Jansen J.D., Luthi S.M., An evaluation of relevant geological parameters for predicting the flow behaviour of channelized reservoirs. Petroleum Geosciences, 15 (4), (2009) 345–354.

De Vault B., Jeremiah J., Tectonostratigraphy of the nieuwerkerk formation (Delfland subgroup) west Netherlands basin. AAPG Bull. 86 (10), (2002)1679–1707.

Energieonderzoek Centrum Nederland (ECN). Eindadvies Basisbedragen SDE+2017, Amsterdam, 2017.

EBN B.V., Hoetz G., de Jong S., Synergie van stranded fields met geothermie & Geothermie mogelijkheden met olie/gas putten na productie. 2013.

Ellison and Clayton, Reservoir simulation improves implementation of midway sunset steamflood. Western Regional meeting, Bakersfield, CA, USA, vol. 29641, SPE (1995).

Flood Y.S., Hampson G.J., Quantitative analysis of the dimensions and distribution of channelized fluvial sandbodies within a large outcrop dataset: Upper Cretaceous Blackhawk Formation, Wasatch Plateau, central Utah U.S.A., Journal of sedimentary research, 85 (4), (2015) 315–336.

Gharbi R.B., Peters E.J., Garrouch A.A., Effect of heterogeneity on the performance of immiscible displacement with horizontal wells, Journal of Petroleum Science and Engineering 18 (1997) 35-47.

Goodyear C.B. Reynolds P.H., Townsley C.L., Woods, Hot water flooding for high permeability viscous oil fields. SPE-35373-MS, SPE/DOE Improved Oil Recovery Symposium, 21-24 April, Tulsa, Oklahoma (1996).

Hajek E.A., Heller P.L., Sheets B.A., Significance of channel-belt clustering in alluvial basins, Geology, 38 (6), (2010) 535–538.

Hamm V., Lopez S., Impact of Fluvial Sedimentary Heterogeneities on Heat Transfer at a Geothermal Doublet Scale. Stanford Geothermal Workshop, Jan 2012, Stanford, United States. SGP -TR-194, 18, (2012).

Issautier B., Viseur S., Audigane P., Le Nindre Y.-M., Impacts of fluvial reservoir heterogeneity on connectivity: implications in estimating geological storage capacity for CO_2. International Journal of Greenhous Gas Control, 20, (2014) 333–349.

Jabbour C., Quintrad M., Betrin H., Robin M., Oil recovery by steam injection: three-phase flow effects J. Pet. Sci. Eng., 16 (1996) 109–130.

Jones A., Doyle J., Jacobsen T., Kjønsvik D., Which sub-seismic heterogeneities influence waterflood performance? A case study of a low net-to-gross fluvial reservoir, Geological Society, 84, (1995) 5–18.

Joshi S. D., Horizontal Well Technology, PennWell Books, (1991).

Junrong L., Rongqiang L., Zhixue S., Exploitation and utilization technology of geothermal resources in oil fields, Proceedings World Geothermal Congress, Melbourne, Australia, (2015).

Larue D.K., Friedmann F., The controversy concerning stratigraphic architecture of channelized reservoirs and recovery by waterflooding, Petroleum Geosciences, 11, (2005)131–146.

Larue D.K., Hovadik J.M., Why is reservoir architecture an insignificant uncertainty in many appraisal and development studies of clastic channelized reservoirs?, Journal of petroleum geology, 31 (4), (2008) 337–366.

Larue D.K., Hovadik J.M., Connectivity of Channelized reservoirs: a modelling approach, Petroleum Geology, 12 (4), (2006) 291–308.

Macenić M., Kurevija T., Revitalization of abandoned oil and gas wells for a geothermal heat exploitation by means of closed circulation: Case study of the deep dry well Pčelić-1.” Interpretation, 6(1), (2018) SB1-SB9.

Milton B.B., Nitzken J.A., Controlling Steam Production in Heat Recovery Steam Generators for combined Cycle and Enhanced Oil Recovery Operations, Power Gen International, Las Vegas, Nevada, December 9-11, 2003.

Nick H.M., Schotting R., Gutierrez-Neri M., Johannsen K., Modeling transverse dispersion and variable density flow in porous media, Transport in Porous Media 78 (1), (2009), 11–35.

Nick, H. M., Wolf, K. H., & Bruhn, D. Mixed CO_2-water injection into geothermal reservoirs: a numerical study. In Proceedings World Geothermal Congress, Melbourne, Australia (2015).

Okasha T.M., Menouar H.K., Abu-Khamsin S.A., Oil recovery from tarmat reservoirs using hot water and solvent flooding, J. Can. Pet. Technol., 37(4), (1998), 33–40.

Pederson J. M., Sitorus J. H., Geothermal hot waterflood: Balam South Telisa Sand, Sumatra, Indonesia, SPE 68724, (2001).

Poulsen, S. E., Balling, N., and Nielsen S. B., A parametric study of the thermal recharge of low enthalpy geothermal reservoirs. Geothermics, 53, (2015), 464–478.

Prats M., Thermal recovery SPE Monogr., 7 (1986).

Pranter, M.J., Ellison, A.I., Cole R.D., Patterson P.E., Analysis and modelling of intermediate-scale reservoir heterogeneity based on a fluvial point-bar outcrop analogue, Williams Fork Formation, Piceance Basin, Colorado. AAPG Bull. 91 (7), 1025–1051.

Pujol, M., Ricard, L. P., and Bolton, G. (2015). 20 years of exploitation of the Yarragadee aquifer in the Perth Basin of Western Australia for direct-use of geothermal heat. Geothermics, 57, (2015), 39–55.

Saeid S., Al-Khoury R., Nick H.M., Hicks M.A., A prototype design model for deep low-enthalpy hydrothermal systems, Renewable Energy, 77 (2015), 408–422.

Salimi H., Wolf K.H., Bruining J., The influence of capillary pressure on the phase equilibrium of the CO_2–water system: Application to carbon sequestration combined with geothermal energy, International Journal of Greenhouse Gas Control, 11 (2012), S47-S66.

Salimzadeh, S., Nick H.M., Zimmerman R.W., Thermoporoelastic effects during heat extraction from low-permeability reservoirs. Energy 142 (2018): 546-558.

Smits P., (2008), Construction of an integrated reservoir model using the Moerkapelle field for geothermal development of the Delft sandstone, MS thesis, Delft University of Technology, Delft, the Netherlands.

Sanner, B., Ria, K., Land, A., Mutka, K., Papillon, P., Stryi-Hipp, G., and Weiss, W. (2011). Common Vision for the Renewable Heating & Cooling sector in Europe. Technical report, European Commission.

Taber J.J., Martin F.D., Serigth R.S., EOR Screening Criteria Revised – Part 1: Introduction to Screening Criteria and enhanced Recovery Field Projects, SPE 35385, WEA, SPE/DOE Improved Oil Recovery Symposium held in Tulsa, Oklahoma, 21-24 April, 1996.

Teodoriu C., Falcone G., Espinel A., Letting Off Steam and Getting into Hot Water - Harnessing the Geothermal Energy Potential of Heavy Oil Reservoirs, Paper presented at the 20th World Energy Congress, (2007) Rome, Italy.

TNO, Nl olie- en gasportaal (1977), www.nlog.nl

Tureyen, O. I., Sarak, H., Altun, G., and Satman, A. (2015). A modeling analysis of unitized production: Understanding sustainable management of single-phase geothermal resources with multiple lease owners. Geothermics, 55:159–170.

Wang X.Z., Wang J.Y., Study on Feasibility of Geothermal Oil Recovery in Gudong Oilfield, FaultBlock Oil & Gas Field, 23(1), (2008), 126- 128.

Willems, C.J., (2017) Doublet deployment strategies for geothermal Hot Sedimentary Aquifer exploitation, PhD thesis, Delft University of Technology, The Netherlands.

Willems, C. J. L., & Nick, H. M., Towards optimisation of geothermal heat recovery: An example from the West Netherlands Basin. Applied Energy, 247 (2019), 582-593.

Willems, C.J., Nick, H.M., Donselaar, M.E., Weltje, G.J. and Bruhn, D.F., On the connectivity anisotropy in fluvial Hot Sedimentary Aquifers and its influence on geothermal doublet performance. Geothermics, 65, (2017a), 222-233.

Willems C.J.L., Nick H.M., Goense T., Bruhn D.F., The impact of reduction of doublet well spacing on the Net Present Value and the life time of fluvial Hot Sedimentary Aquifer doublets, Geothermics, 68, (2017b), 54–66.

Willems, C.J., Nick, H.M., Weltje, G.J. and Bruhn, D.F., An evaluation of interferences in heat production from low enthalpy geothermal doublets systems, Energy, 135 (15), (2017c), 500-512.

Willis B.J., Tang H., Three-dimensional connectivity of point-Bar deposits, Journal of sedimentary research, 80 (5), (2010) 440–454.

Wys J.N., Kimmell C.E., Hart, G.F., The feasibility of recovering medium to heavy oil using geopressured geothermal fluids, Prepared for US Department of Energy, Field Office, Idaho, (1991).

Van Heekeren V., The Netherlands Country Update on Geothermal Energy, Stichting Platform Geothermie, World Geothermal Congress (2015).

Van Wees JDAM, Kramers I, Kronimus RA, Pluymaekers MPD, Mijnlieff HF, Vis GJ. ThermoGis V1.0, Part II: methodology. 2010. TNO-Report.

Verney, M. J., Evaluating SAGD Performance due to Changes in Well Spacing and Length, SPE 174481-MS, (2015).

Vik, H. S., Salimzadeh, S., & Nick, H. M., Heat recovery from multiple-fracture enhanced geothermal systems: The effect of thermoelastic fracture interactions. Renewable energy, 121 (2018), 606-622.

Zhao D.W., Wang J., Gates I.D., Thermal recovery strategies for thin heavy oil reservoirs, Fuel, 117, (2014) 431–441.

Ziabakhsh-Ganji Z., Kooi H., Sensitivity of Joule–Thomson cooling to impure CO_2 injection in depleted gas reservoirs, Applied Energy, 113, (2014) 434–451.

Ziabakhsh-Ganji Z., Donselaar M.E., Bruhn D.F., Nick H.M., Thermally-enhanced oil recovery from stranded fields: Synergy potential for geothermal and oil exploitation, European geothermal congress, Strasburg, France, (2016).

Ziabakhsh-Ganji Z., Nick H.M., Donselaar M.E., Bruhn D.F., Synergy potential for oil and geothermal energy exploitation, Applied Energy, 212, (2018) 1433–1447.

Appendix I

For a geothermal system with a rigid rock, incompressible fluids and local thermal equilibrium between rock and fluid the heat transfer equation including conduction and convection processes can be written as:

$$\frac{\partial(\rho CT)}{\partial t} = \nabla.(\boldsymbol{\lambda}\nabla T) - \nabla.\left(\rho_f C_f \boldsymbol{u} T\right) - \rho_f C_f q' T' \tag{A-1}$$

where t is time [s], T the temperature [K], $\boldsymbol{\lambda}$ the total conductivity tensor [W/(mK)], ρ_f the fluid density [kg/m3], C_f the fluid specific heat capacity [J/(kgK)], $\boldsymbol{u}$ is Darcy velocity vector [m/s], and ρC is the volumetric heat capacity, q' is external sinks and sources [1/s], and T' refers to the temperature at sources/sinks. Darcy velocity is calculated as: $\boldsymbol{u} = -k/\mu\nabla P$, where μ is the dynamic viscosity [Pa s], k is permeability [mD] and P is the fluid pressure [Pa]. The fluid pressure field can be obtained by combining of the continuity and Darcy equations as:

$$\emptyset\frac{\partial(\rho_f)}{\partial t} + \nabla.\left(\rho_f \frac{k}{\mu}\nabla P\right) = \rho_f q^* \tag{A-2}$$

The total thermal conductivity is expressed as: $\boldsymbol{\lambda} = \lambda_{eq}\boldsymbol{I} + \boldsymbol{\lambda}_{dis}$. Where λ_{eq} is the equivalent conductivity of the fluid and the matrix and the $\boldsymbol{\lambda}_{dis}$ the thermal dispersion tensor. This equivalent conductivity and the volumetric heat capacity are both volumes averaged:

$$\lambda_{eq} = (1-\phi)\lambda_s + \phi\lambda_f \tag{A-3}$$

$$\rho C = (1-\phi)\rho_s C_s + \phi\rho_f C_f \tag{A-4}$$

where the suffixes s and f stand for solid (shale, sand) and fluid (brine), respectively. The thermal dispersion tensor, which is based on the solute dispersion model, may be written as:

$$\boldsymbol{\lambda} = \left(\lambda_{eq} + (\alpha_T|\boldsymbol{u}|)\right)\boldsymbol{I} + \rho_f C_f(\alpha_L - \alpha_T)\frac{\boldsymbol{uu}}{|\boldsymbol{u}|} \tag{A-5}$$

where $|\ \boldsymbol{u}\ |$ is the magnitude of the Darcy velocity vector and α_L and α_T are the thermal dispersion coefficients in the longitudinal and transversal direction, respectively. The viscosity of the brine (the geothermal fluid) varies with temperature (T) and the salinity (S_a) of the brine [ppm/10^6] as:

$$\mu = 0.1 + 0.333S_a + \left(1.65 + 91.9{S_a}^3\right)e^{\left\{-\left[0.42\left({S_a}^{0.8}-0.17\right)^2+0.045\right]T^{0.8}\right\}} \tag{A-6}$$

The density of the brine depends on the temperature, the pressure and the salinity (S_a) as:

$$\begin{aligned}\rho_f = \rho_w + S_a\{&0.668 + 0.44S_a \\ &+ 10^{-6}\left[300P - 2400PS_a\right. \\ &\left.+ T\left(80 + 3T - 3300{S_a}^3P + 47PS_a\right)\right]\}\end{aligned} \tag{A-7}$$

where

$$\rho_w = 1 + 10^{-6}(-80T - 3.3T^2 + 0.00175T^3 + 489P - 2TP + 0.016T^2P - 1.3 \times 10^{-5}T^3P - 0.333P^2 - 0.002TP^2) \quad \text{(A-8)}$$

For equations A-6, A-7 and A-8, T is in [°C] and P in [MPa].

Tables

Table 1: List of parameters used in the geothermal model Domain 1

Parameters	Value	Dimension	Description
T_0	100	°C	Initial reservoir temperature
T_{inj}	37	°C	Injection cold water temperature
P_0	20	MPa	Initial reservoir pressure
Cp_f	4200	J/(kg K)	Specific heat capacity of the fluid
λ_f	0.67	W/(m K)	Conductivity of the pore fluid
S	0.02	ppm/10^6	Salinity of the injection fluid
α_T	0.001	m	Transversal dispersion coefficient
α_L	0.01	m	Longitudinal dispersion coefficient
r_w	0.075	m	Wellbore radius
ϕ_{res}	0.28	-	Porosity
λ_s	3	W/(m K)	Conductivity of the reservoir rock
ρ_s	2650	kg/m^3	Density of the reservoir rock
Cp_s	980	J/(kg K)	Specific heat capacity of the reservoir rock
k_{res}	1000	mD	Permeability of the reservoir
Adjacent layer (over- and underburden)			
ρ_{adj}	2600	kg/m^3	Density of the adjacent (over and underburden) rock
λ_{adj}	2.0	W/(m K)	Conductivity of the rock
Cp_{adj}	950	J/(kg K)	Specific heat capacity of the rock
ϕ_{adj}	0.05	-	Porosity
k_{adj}	0.01	mD	Permeability

Table 2. Oil reservoir Domain (2) sand body geometries (Crooijmans et al., 2016)

Sand body geometries	
Bank-full flow width	40 m
Bank-full flow depth	4 m
Meander belt width	800-1200 m
Single-story sandstone body thickness	4-5 m
Single-story sandstone body width	200-400 m
Multi-story sandstone thickness	6-20 m
Multi-story sandstone width	100-500
Width/thickness ratio sandstone bodies	16-100

Table 3. Oil viscosity for different heavy oil reservoirs (Alajmi et al., 2014)

Oil viscosity				
Temperature (°C)	**Coalinga**	**Cymric**	**KernRiver**	**Moerkapelle**
35	503.8448	13318.65	852.0764	1026.069
40	368.1943	9397.877	687.4707	723.111
50	184.0971	2913.142	319.5286	390.1115
60	96.89323	1117.37	164.6057	229.1526
70	58.13594	508.8023	96.82686	143.5647
100	18.50661	85.79803	25.75595	46.07246
135	7.073206	23.34505	9.682686	16.84984
177	3.29437	8.599756	4.260382	6.588901

Table 4: Variables used in the NPV calculation of the Geothermal and EOR sides of the synergy. CAPEX and fixed OPEX are calculated with the capacity of the installations, while variable OPEX is calculated with the actual output of the system (Ziabakhsh-Ganji et al., 2018).

Geothermal side		
item	*value*	*unites*
CAPEX	1622	Euro/kW (capacity)
Fixed OPEX	59	Euro/kW/year (capacity)
Variable OPEX	0.008	Euro/kWh/year (output)
EOR side		
item	*value*	*unites*
CAPEX	Eq.14	Total for two wells drilling, pump energy and also well stimulation*
Fixed OPEX	3%	of cumulative CAPEX/year
Variable OPEX	11.45	Euro/sm3 (oil)
Oil Evacuation costs	11.45	Euro/sm3 (oil)

*The CAPEX is developed based on Van Wees et al. (2010) method.

Figures:

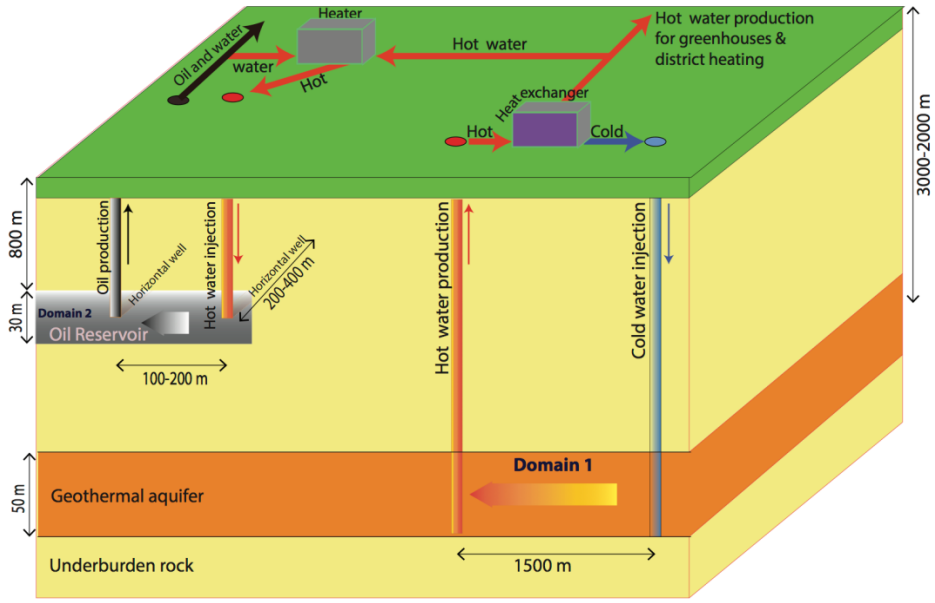

Figure 1: Schematic of the conceptual model and simulation study domains. The arrows next to the wells represent the flow direction. The geothermal well distance is 1500 m while different well distances ranging from 100 m to 200 m are examined for Domain 2.

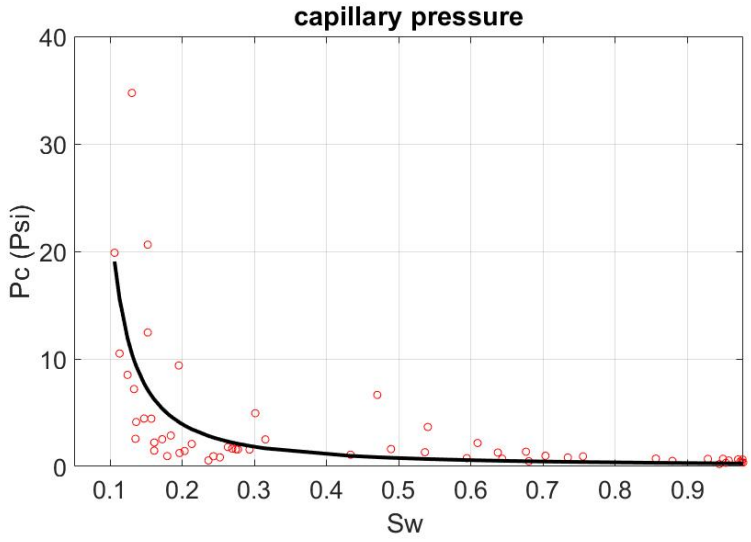

Figure 2: Capillary pressure versus water saturation. The line is derived from model calculations based on the Brooks-Corey correlation, and symbols are experimental data.

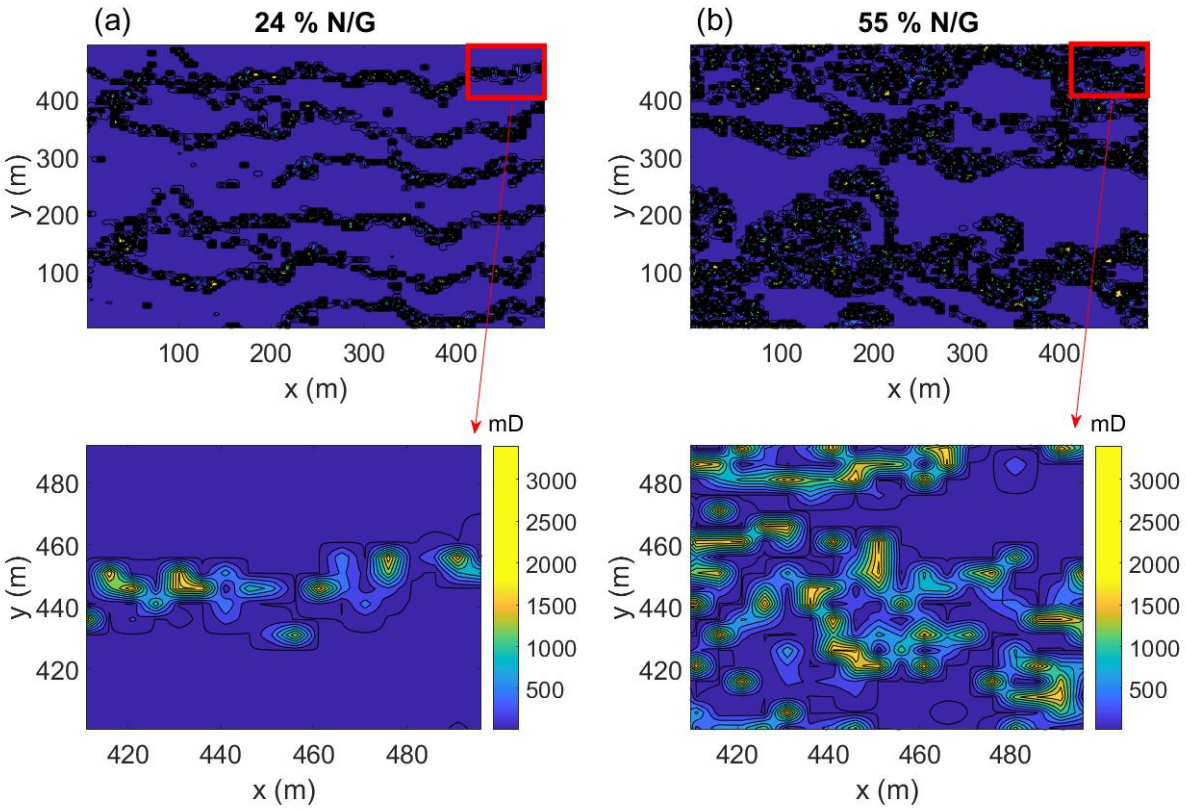

Figure 3: Permeability distributions in the model. The permeability varies from 5 mD for non-reservoir (blue) bodies to 3500 mD for reservoir (dark) bodies.

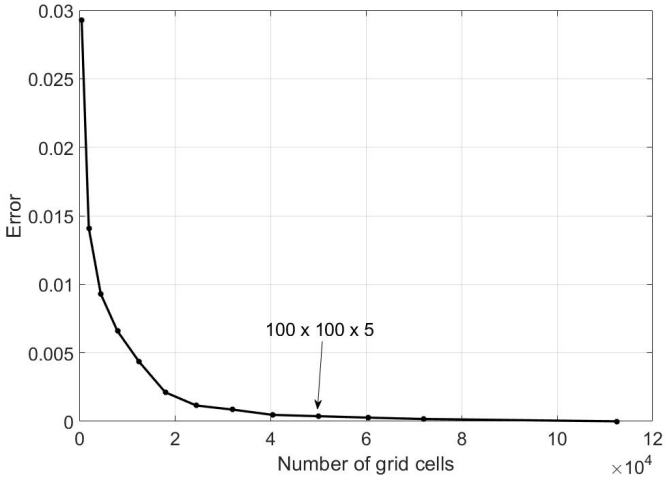

Figure 4: Schematic of the grid sensitivity analysis for the oil reservoir. 50000 grid cells are sufficient for this study.

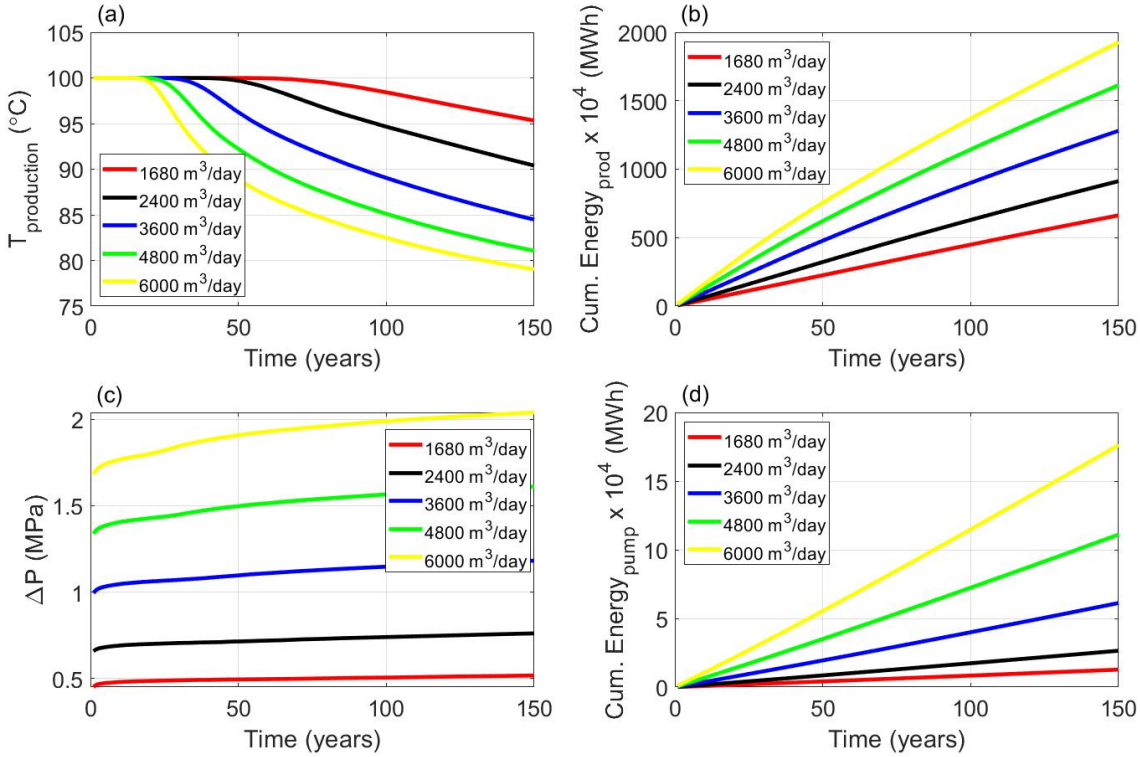

Figure 5: Results for the geothermal domain when various discharges contribute to a) production temperature, b) cumulative energy production, c) pressure drop (injection well pressure minus production well pressure) and d) cumulative energy consumption for pumping.

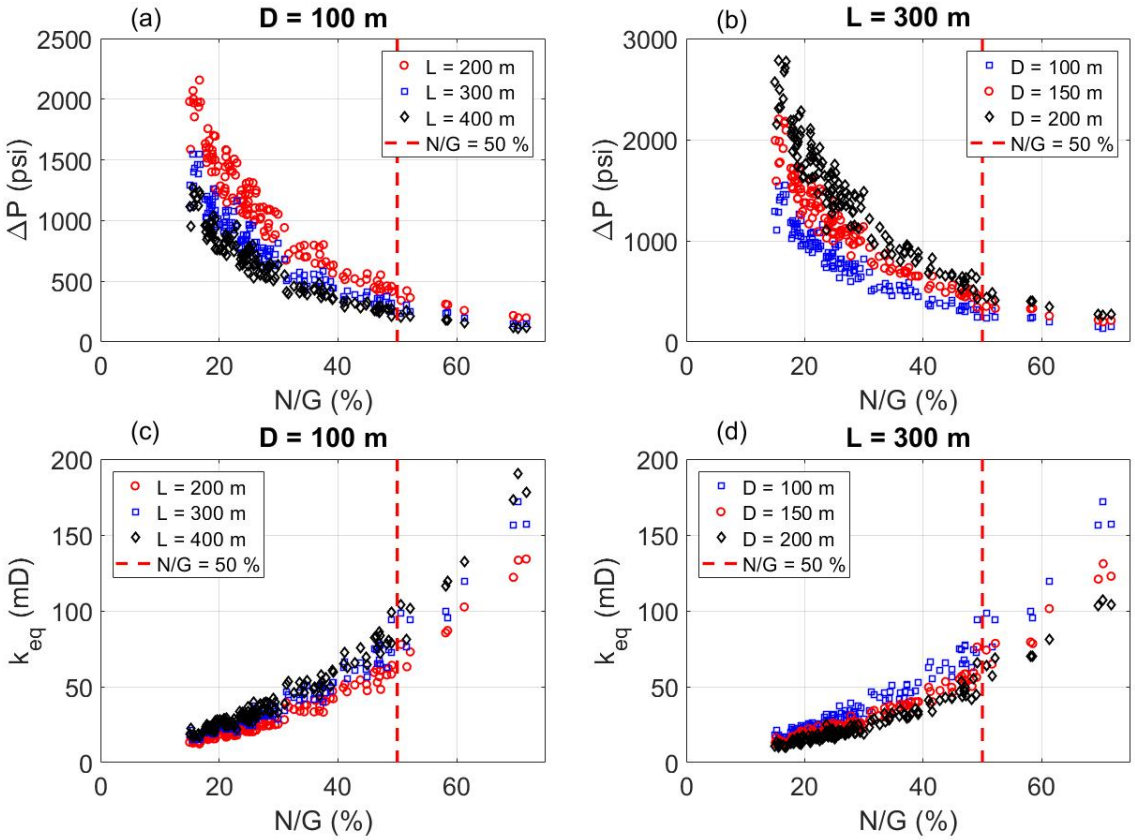

Figure 6: Effect of N/G on pressure drop and on the equivalent permeability K_{eq} in the oil domain reservoir for various horizontal wellbore configurations, when the fluid flow through the reservoir is single phase.

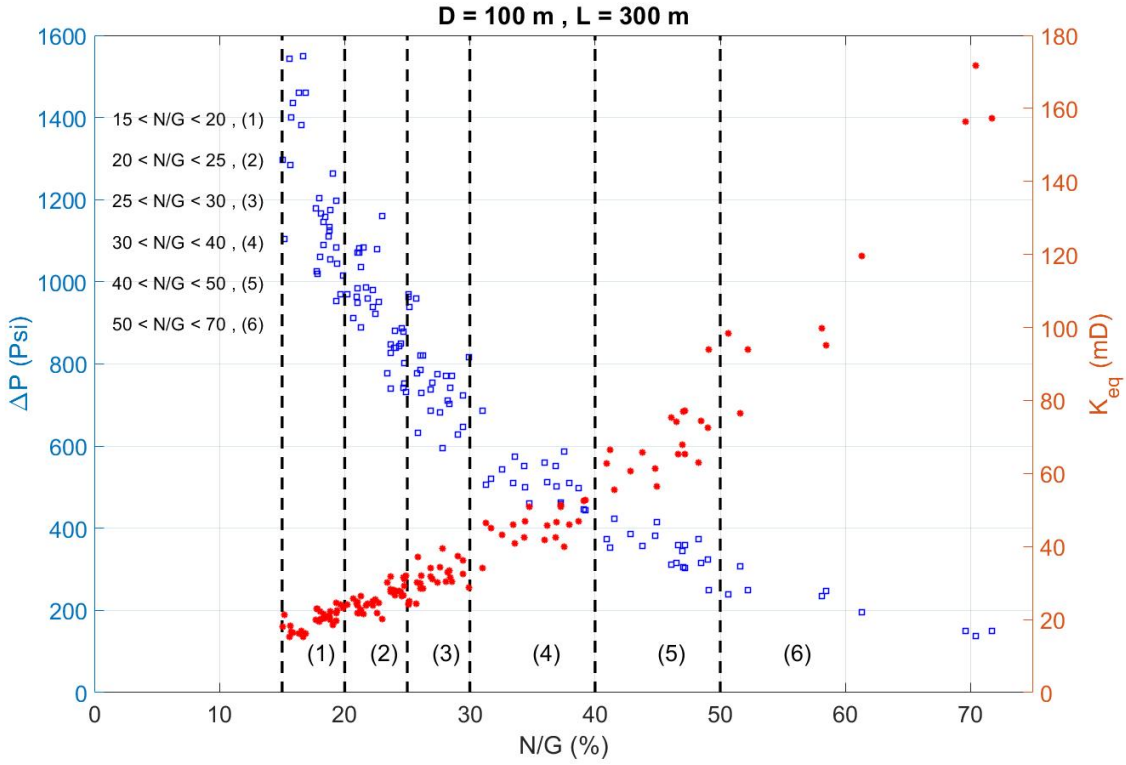

Figure 7: Clustering the models in 6 groups based on N/G. Red and blue symbols indicate the K_{eq} and pressure drop respectively for different N/G. Note that the clustering derived from the average pressure drop is about 200 psi. However, the pressure drop for cluster (1) is higher than 200 psi.

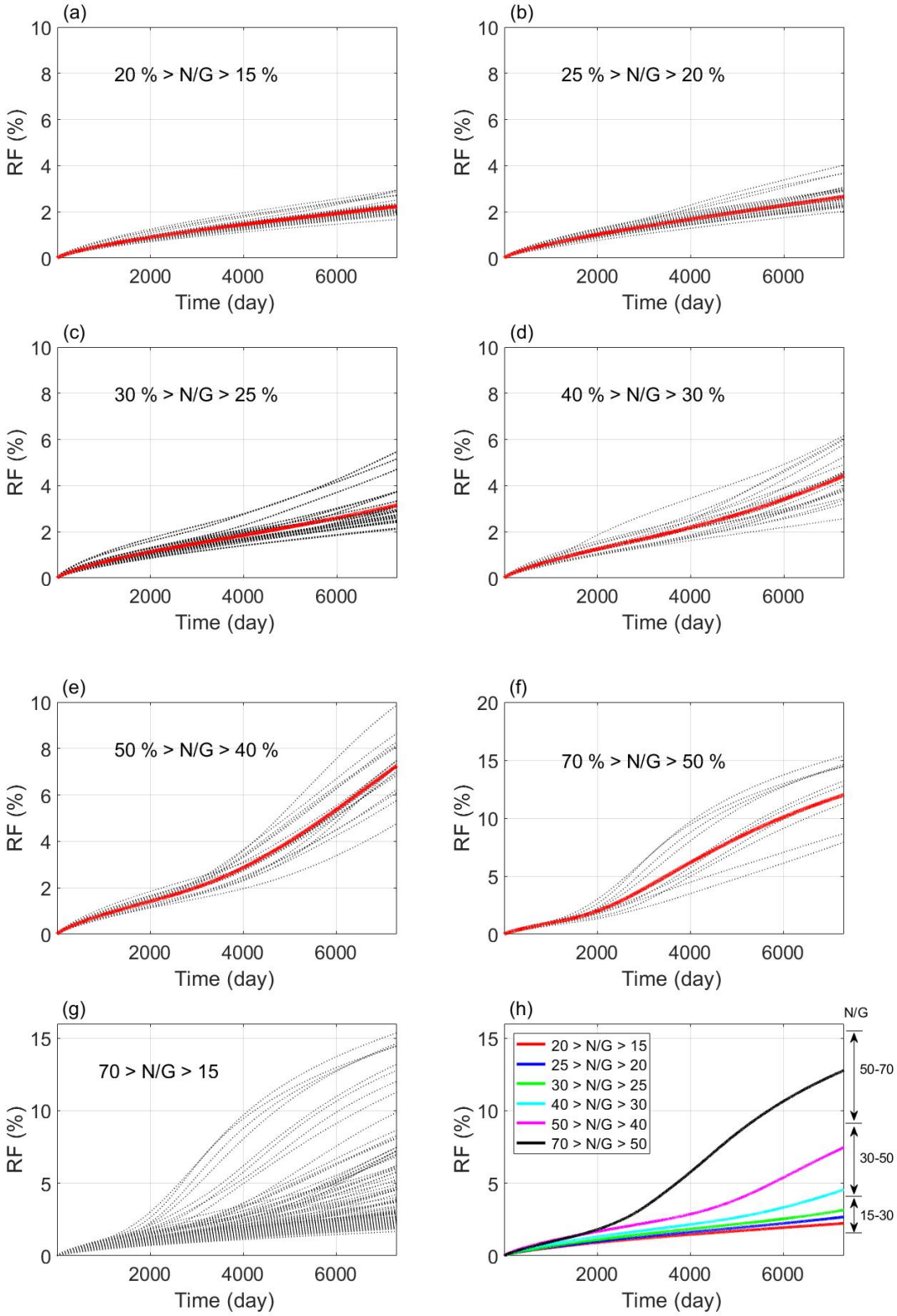

Figure 8: Effect of N/G on oil recovery factor (RF) when injection temperature, well length (L) and well spacing (D) are 100 °C, 300 m and 100 m respectively. In (a) to (f) the red lines indicate the average realization of each cluster. (g) indicates the RF for entire range of N/G.

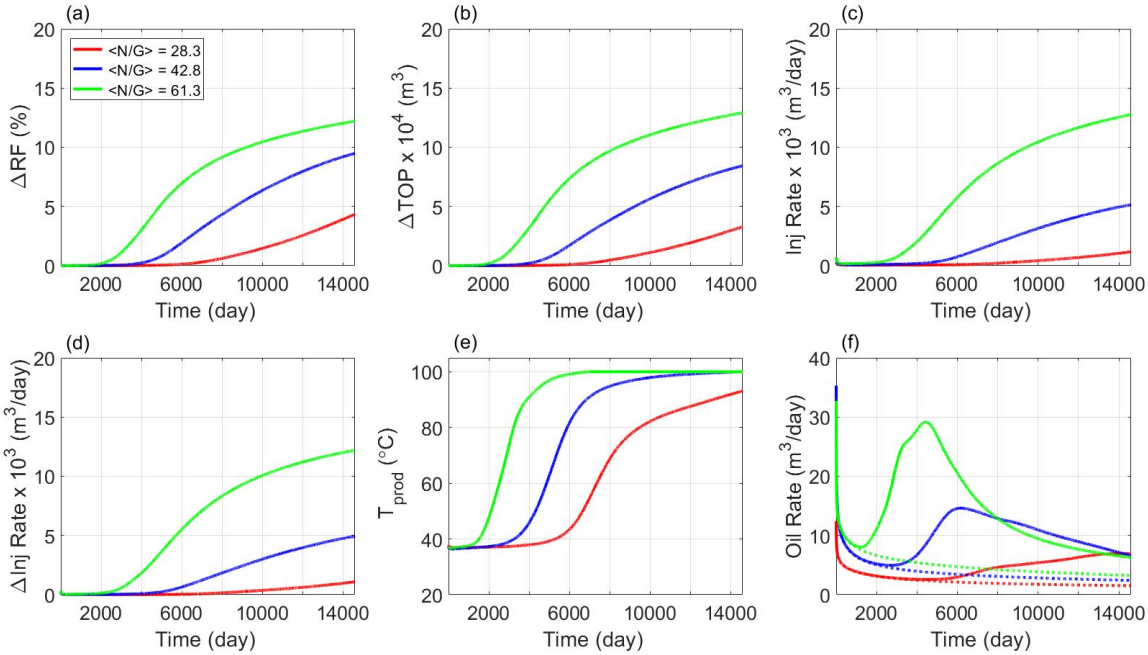

Figure 9: Effect of N/G on a) ΔRF, b) ΔTOP, c) injection rate at 100 °C, d) ΔInj rate, e) temperature profile of oil production well and f) daily oil production rate when well length (L), well spacing (D), and BHP are 300m, 100 m and 1669 psi respectively. The ΔInj rate indicate the injection rate difference between conventional water flooding (the injected water temperature (37 °C) similar to that of the oil reservoir) and hot water flooding (100 °C).

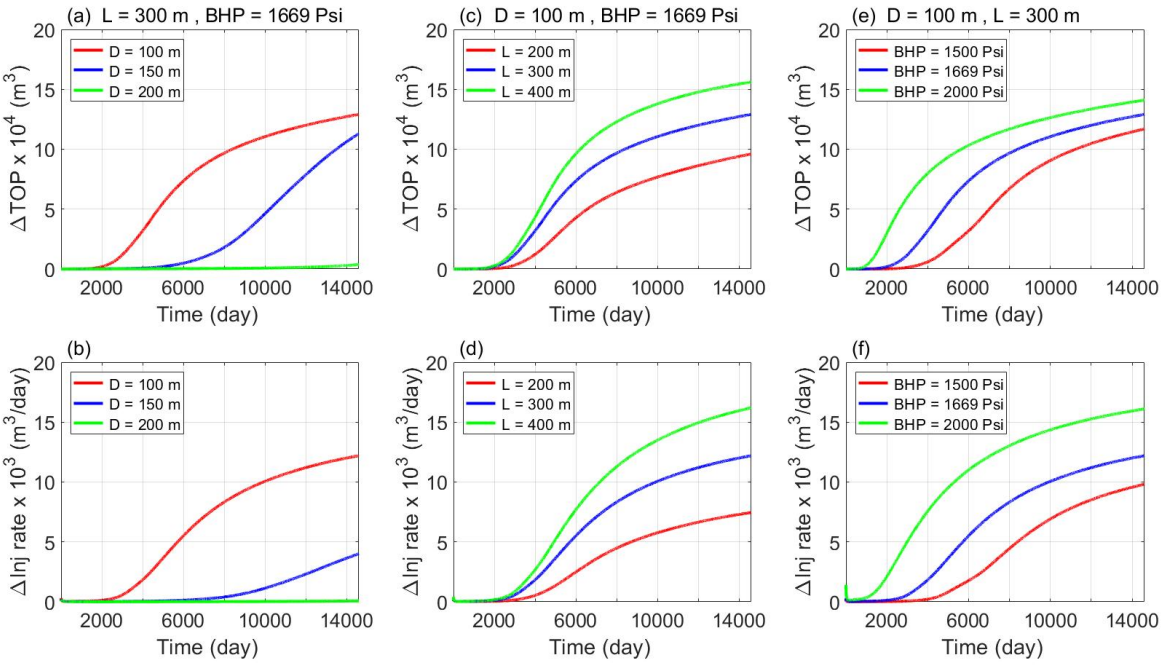

Figure 10: Effect of (a, b) well distance, (c, d) well length (L) and (e, f) BHP on ΔTOP and ΔInj rate when N/G is 63.2%.

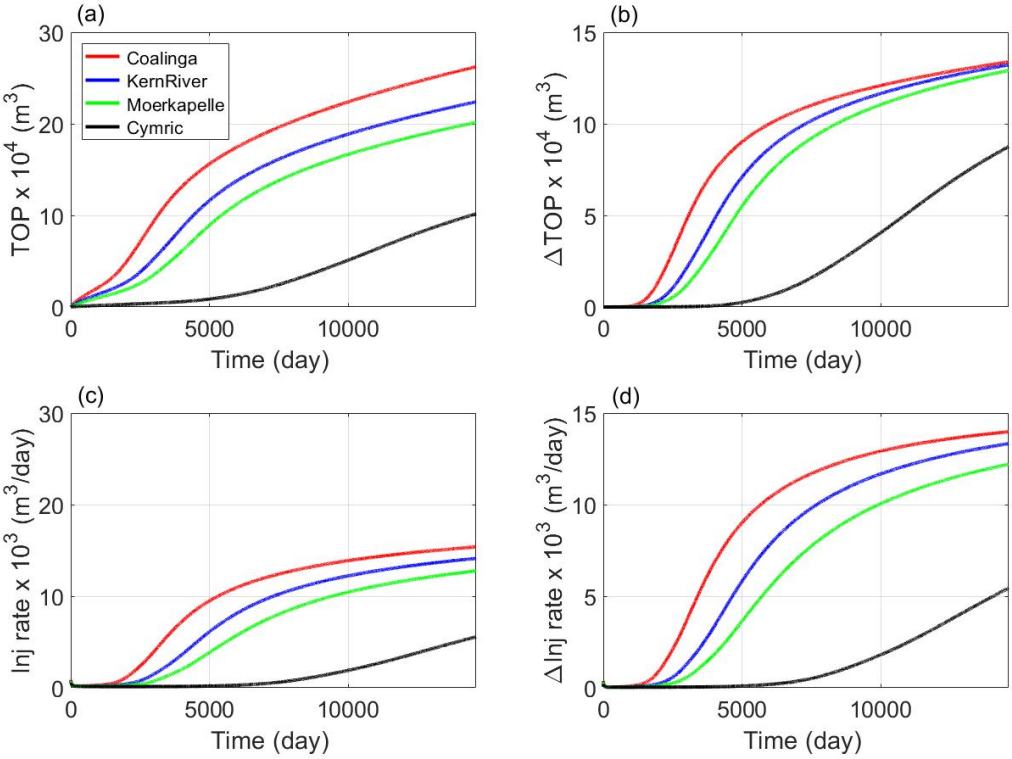

Figure 11: Effect of various oil viscosities on a) TOP, b) ΔTOP c) injection rate d) ΔInj rate when injection temperature is 100 °C, N/G = 61.3 %, L = 300 m, D = 100 m and BHP = 1669 Psi.

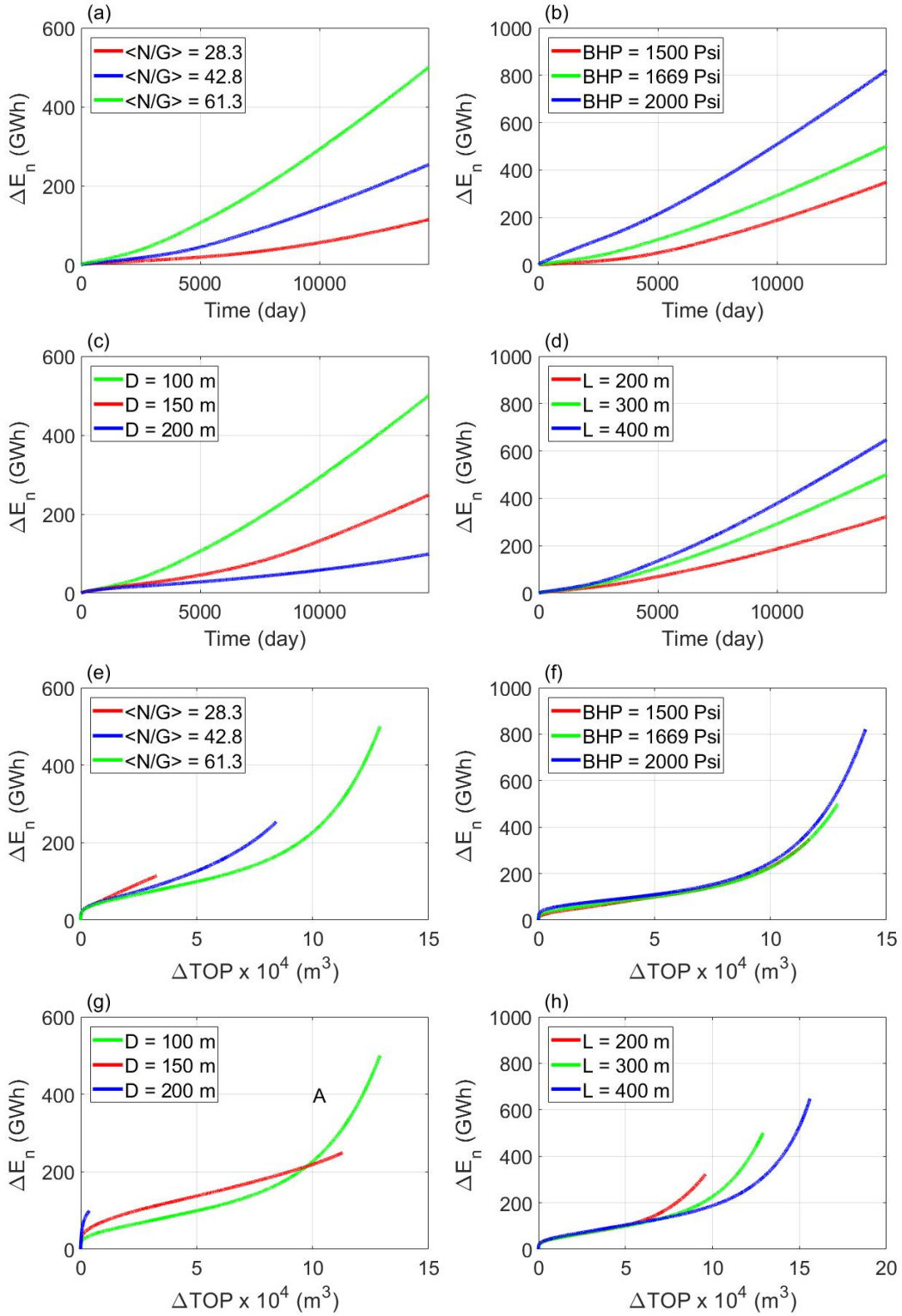

Figure 12: (a) – (d): Results of total consumed energy with time of simulation for a) various N/Gs when D = 100 m, L = 300 m, BHP = 1669 Psi b) various BHP when D = 100 m, L = 300 m, N/G = 61.3 % , c) different wellbore spacing when L = 300 m, BHP = 1669 Psi, N/G = 61.3 % , d) various wellbore lengths when D = 100 m, BHP = 1669 Psi, N/G = 61.3 %. (e) – (h) show the results of total consumed energy versus ΔTOP for the same scenarios as those mentioned in (a) to (d).

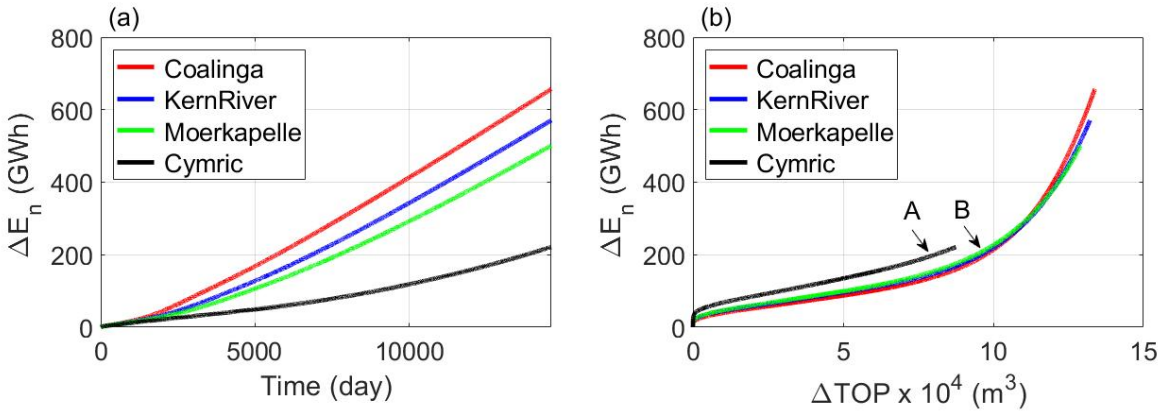

Figure 13: Difference in total consumed Energy for various oil viscosities when D = 100 m, L = 300 m, N/G = 61.3 %, BHP = 1669 Psi and injection temperature is 100 °C.

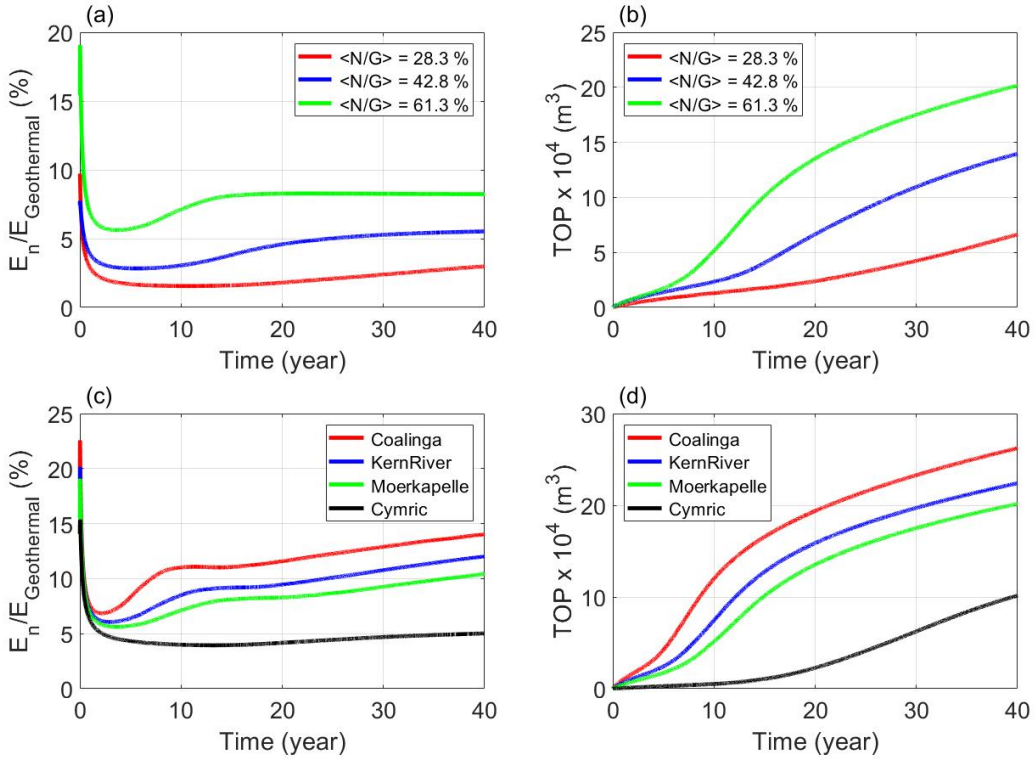

Figure 14: The ratio of consumed cumulative energy (E_n) per cumulative produced geothermal energy for various scenarios for 40 years of hot water flooding of 100 °C.

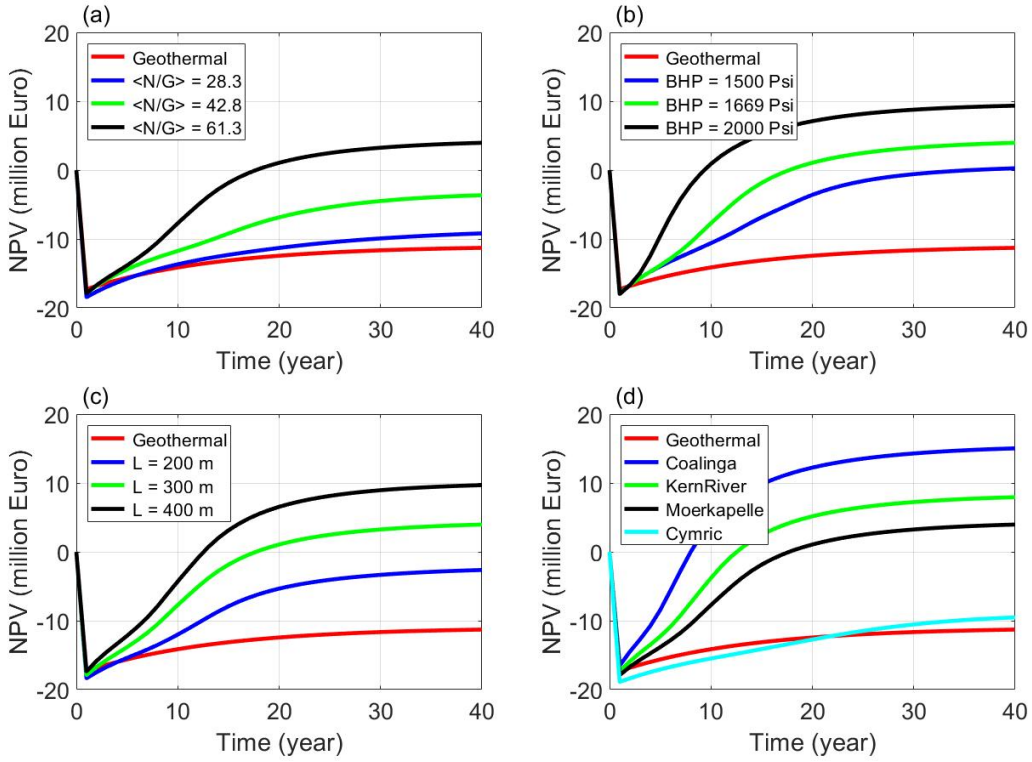

Figure 15: NPV calculations for various scenarios in this study when energy production from oil reservoir is included and hot water injection temperature is 100 °C. Note that the red lines show the NPV for a single geothermal doublet.